Remote Sensing of Environment 264 (2021) 112615

Contents lists available at ScienceDirect

Remote Sensing of Environment

journal homepage: www.elsevier.com/locate/rse

Towards user-adaptive remote sensing: Knowledge-driven automatic classification of Sentinel-2 time series

Damien Arvor [a,*], Julie Betbeder [b,c,d], Felipe R.G. Daher [a], Tim Blossier [a], Renan Le Roux [b,c], Samuel Corgne [a], Thomas Corpetti [a], Vinicius de Freitas Silgueiro [e], Carlos Antonio da Silva Junior [f]

[a] CNRS, UMR 6554 LETG, Université Rennes 2, 35043 Rennes, France
[b] CIRAD, Forêts et Sociétés, F-34398 Montpellier, France
[c] Forêts et Sociétés, Univ Montpellier, CIRAD, Montpellier, France
[d] Unidad de Acción Climática, CATIE - Centro Agronómico Tropical de Investigación y Enseñanza, 30501 Turrialba, Costa Rica
[e] ICV, Instituto Centro de Vida, 3473 Ariosto da Riva Ave, 78580000, Alta Floresta, Brazil
[f] UNEMAT, State University of Mato Grosso, Department of Geography, 78555000 Sinop, Mato Grosso, Brazil

ARTICLE INFO

Editor: Marie Weiss

Keywords:
Land cover
Sentinel-2
Time series
Knowledge-driven
Ontologies
Amazon

ABSTRACT

Land cover mapping over large areas is essential to address a wide spectrum of socio-environmental challenges. For this reason, many global or regional land cover products are regularly released to the scientific community. Yet, the remote sensing community has not fully addressed the challenge to extract useful information from vast volumes of satellite data. Especially, major limitations concern the use of inadequate classification schemes and "black box" methods that may not match with end-users conceptualization of geographic features. In this paper, we introduce a knowledge-driven methodological approach to automatically process Sentinel-2 time series in order to produce pre-classifications that can be adapted by end-users to match their requirements. The approach relies on a conceptual framework inspired from ontologies of scientific observation and geographic information to describe the representation of geographic entities in remote sensing images. The implementation consists in a three-stage classification system including an initial stage, a dichotomous stage and a modular stage. At each stage, the system firstly relies on natural language semantic descriptions of time series of spectral signatures before assigning labels of land cover classes. The implementation was tested on 75 time series of Sentinel-2 images (i.e. 2069 images) in the Southern Brazilian Amazon to map natural vegetation and water bodies as required by a local end-user, i.e. a non-governmental organization. The results confirmed the potential of the method to accurately detect water bodies (F-score = 0.874 for bodies larger than 10 m) and map natural vegetation (max F-score = 0.875), yet emphasizing the spatial heterogeneity of accuracy results. In addition, it proved to be efficient to provide rapid estimates of degraded riparian forests at watershed level (R^2 = 0.871). Finally, we discuss potential improvements both in the system's implementation, e.g. considering additional characteristics, and in the conceptual framework, e.g. moving from pixel- to object-based image analysis and evolving towards a hybrid system combining data- and knowledge-driven approaches.

1. Introduction

Monitoring land cover dynamics is essential to address a wide spectrum of challenges related to climate change, health and well-being, food safety or environmental degradation such as listed by the United Nations through the Sustainable Development Goals (SDG) (Sachs, 2012). The scientific community needs manageable spatio-temporal indicators to monitor the achievement of these SDGs (Hák et al., 2016). In this regard, the remote sensing science is expected to play an essential role (CEO, 2018), contributing actively to the more general land change science that seeks to understand the land cover/land use dynamics as a coupled human-environment system (Turner et al., 2007). Yet, the task is challenging since end-users require spatial information at ever larger scale (e.g. regional to global scale), shorter time intervals (e.

* Corresponding author.
E-mail address: damien.arvor@univ-rennes2.fr (D. Arvor).

https://doi.org/10.1016/j.rse.2021.112615
Received 12 February 2021; Received in revised form 18 July 2021; Accepted 19 July 2021
Available online 4 August 2021
0034-4257/© 2021 The Authors. Published by Elsevier Inc. This is an open access article under the CC BY-NC-ND license (http://creativecommons.org/licenses/by-nc-nd/4.0/).

g. annually or even more frequently) and higher spatial resolution to monitor ever finer land change dynamics (Cerbaro et al., 2020a) (e.g. mapping agricultural practices (Bégué et al., 2018) or forest degradation (Bullock et al., 2020; Câmara, 2020)).

For this purpose, the remote sensing community has released many ready-to-use global or regional maps to serve as input for other scientists interested in land change sciences (e.g. climatology, health sciences, agronomy, ecology, geography, etc). While coarse resolution maps (250 m to 1 km) have been considered inadequate for global change studies and for resource management (Giri et al., 2013; Rocchini et al., 2013), higher resolution large-scale remote sensing-based maps have been produced recently and their quality discussed in numerous scientific papers. For example, the Global Forest Change (Hansen et al., 2013), the Global Surface Water (Pekel et al., 2016), the FROM-GLC (Gong et al., 2013) and the GlobeLand30 (Chen et al., 2015) products are global-scale maps of forest, water and land cover dynamics, respectively, at 30 m resolution. These breakthrough experiences were also completed by regional initiatives such as, among others, the Corine Land cover maps in Europe (Büttner, 2014), the French land use maps based on Landsat-8 and Sentinel-2 time series (Inglada et al., 2017), the South American Landsat-based land cover maps (Giri and Long, 2014), the Brazilian initiatives for land cover mapping at national (Souza et al., 2020) and regional scale (Bullock et al., 2020; de Almeida et al., 2016; Souza et al., 2019).

But despite these great advances, the remote sensing community has not yet fully addressed the challenge to extract useful information from vast volumes of satellite data so that current regional and global land cover products still present major conceptual limitations (Congalton et al., 2014; Grekousis et al., 2015; Arvor et al., 2019). Below, we introduce some of these limitations regarding the use of inadequate classification schemes and data-driven approaches with regard to the end-users requirements.

1.1. Inconsistencies between classification schemes and end-users requirements

The first major limitation refers to the choice of an adequate classification scheme. All land cover maps are based on a priori defined class labels such as"Forest formations" (Souza et al., 2020),"Primary Forested Natural Vegetation" (de Almeida et al., 2016),"Forests" (Giri et al., 2013) or"Forest" (Chen et al., 2015). Each of these labels usually refers to one explicit definition so that the classification schemes turn to be very static. This is an issue since the maps are designed to be used by a wide community of users (Cerbaro et al., 2020b), who have their own conceptualizations of geographic concepts and their own final objectives. In this regard, using static classification schemes forces the user to adapt its own conceptualization to the map producer's conceptualization.

In addition, there are often inconsistencies between the class descriptions and the real capacity of remote sensors to map them. This issue is referred to as the sensory gap, i.e. the gap between the entity in the world and the information in a (computational) description derived from a recording of that scene (Smeulders et al., 2000). For example, the definition of the"Forests" class in Giri and Long (Giri and Long, 2014) refers to"plants, 3 m or greater in height" although the Landsat images used to produce the maps cannot measure vegetation height. Congalton et al. (Congalton et al., 2014) also pointed out this problem regarding standard classification schemes such as the Land Cover Classification System (LCCS (Di Gregorio, 2005)), i.e. a reference classification scheme used in various mapping efforts such as the AfriCover project (Kalensky, 1998) or the South America land cover map (Giri and Long, 2014). They emphasized that the LCCS is based on inference rules using ecological or environmental criteria, which cannot all be identified from optical remotely sensed imagery (e.g. vegetation height, number of layers in vegetated areas, etc) (Congalton et al., 2014).

Besides the sensory gap, the semantic gap is the lack of agreement between the information that one can extract from the visual data and the interpretation made of the same data by a user in a given situation (Smeulders et al., 2000). In other words, it describes the gap between the low-level information contained in an image (e.g. reflectance values assigned to pixels) and the high-level semantic concepts used to interpret the image (Arvor et al., 2019). As an example, the semantic gap is emphasized in remote sensing when complex features (e.g. a"urban" or"forest" area) are represented by different spectral signatures (Jensen, 1983), thus making them difficult to map in pixel-based land cover products using the sole spectral information. Of course, depending on the comprehensiveness of the training dataset, advanced supervised classifiers can deal with such complex classes, e.g. by assigning the"-urban" class to different spectral signatures classified in different branches of a decision tree. But, in the case when two leaves of a decision tree have the same label, the interpretability of the classification model turns to be very complex, which tends to widen the semantic gap between the numeric information contained in the pixels and its thematic interpretation.

1.2. Inconsistencies between data-driven methods and end-users requirements

The second major issue is related to the methodological approach applied to produce land cover maps. Here, we differentiate"data-driven" from"knowledge-driven" methods."Data-driven" refers to methods that depend on the data that has been collected. In remote sensing, both supervised and unsupervised classifications can be considered as"data-driven" as they depend on the image and on the training (for supervised classifiers) datasets. In other words, if you change the training data or the EO data, you also change the classification model. In opposition,"knowledge-driven" approaches depend on a priori expert knowledge and are thus independent from the data. For example, it is widely agreed by the remote sensing community that high reflectances in the near infrared (NIR) wavelengths are associated to vegetated land cover. Thus, the corresponding classification model (e.g."high NIR values refer to vegetation cover") is valid for all optical remote sensing data with a NIR band.

In remote sensing, the main effort to promote knowledge-driven approach has been through Geographic Object-Based Image Analysis (GEOBIA (Blaschke et al., 2014; Blaschke, 2010)). Indeed, GEOBIA was initially designed to rely on descriptive assessment and knowledge, i.e. the approach was developed to incorporate the wisdom of the user (Blaschke and Strobl, 2001). In that regard, GEOBIA is characterized by the transformation of knowledge (Lang, 2008) and can be considered as a computer-aided photo-interpretation process (Arvor et al., 2013). Yet, in practice, GEOBIA presents major limitations. Mainly, GEOBIA includes a fully data-driven image segmentation and an object classification stage based on rules that are usually defined through"trial-and-error" analysis or supervised classifiers and can thus also be considered as data-driven. From that perspective, GEOBIA may actually be considered as a hybrid knowledge- and data-driven classification approach restricted to local studies and difficult to transfer and automate for large-scale applications (Lucas et al., 2007; Lucas et al., 2015; Adamo et al., 2020).

Thus, although a few products rest, at least partially, on visual interpretation tasks (GlobeLand30 (Chen et al., 2015), TerraClass (de Almeida et al., 2016), Corine Land Cover (Büttner, 2014)), most studies dedicated to global or regional land cover mapping are based on data-driven approaches (Grekousis et al., 2015). Most high-resolution products rely on supervised classification algorithms (Inglada et al., 2017; Giri and Long, 2014; Souza et al., 2020; Waldner et al., 2015) which excel at perceptual classification, i.e. to identify all pixels in an image that resemble to annotated training samples. In this regard, the last decade has been marked by the rapid emergence of ever more efficient classification algorithms like Support Vector Machines (Mountrakis et al., 2011), Random Forest (Belgiu and Dragut, 2016) or, more

recently, Deep Learning (Zhu et al., 2017). However, these approaches also present important limitations.

First, supervised algorithms require many training data, which is a severe issue since it can induce heterogeneity in the final products depending on the availability and reliability of reference data collected through field campaigns, crowd-sourcing initiatives (Fritz et al., 2012; See et al., 2016) or very high resolution maps (based on UAVs for example (Alvarez-Vanhard et al., 2020)). This assertion is especially valid for Southern countries where major land use changes are expected to occur.

Second, supervised classifiers are often used to produce maps where classes are mutually exclusive with discrete boundaries separating each other. Such approach is not adapted to the monitoring of vague and ambiguous geographic concepts such as vegetation gradients or urban areas. Indeed, the conversion of continuous quantitative information (i.e. spectral signatures) into discrete classes induces a loss of information or leads to an unrealistic representation of reality that may not suit with requirements for ecosystem monitoring (Rocchini et al., 2013). Similarly, Kennedy et al. (Kennedy et al., 2014) note that remote sensing approaches based on static representations of geographic entities mainly allow detecting occasional dramatic disruptions (e.g. deforestation) but are limited to capture continuous changes (e.g. degradation). Yet, it is worth noting that some supervised approaches can also provide a relevant continuous information for the monitoring of spatial gradients and fine temporal changes. However, these estimates derived from optical imagery suffer from a lack of interpretability (e.g. the probability of belonging to a given land cover class does not correspond to any physical reality on the ground) and/or from the sensory gap (see Section 1.1) since optical sensors do not enable direct measurement of variables such as the percent tree cover in Global Forest Change (Hansen et al., 2013) or the fraction of vegetation cover in Copernicus FCover product (Fuster et al., 2020)).

Third, and most importantly from our perspective, supervised classifiers are inefficient to deal with symbolic systems based on inference and abstraction (Marcus, 2018). In data-driven approaches, the knowledge corresponding to a land cover/land use class is a"numeric knowledge" expressed in classification models (e.g. random forest model) which suffers from a lack of interpretability (Small, 2020) whereas most end-users (e.g. geographers, ecologists, agronomists, etc) are used to work with abstract semantic definitions of geographic features (Arvor et al., 2019). For instance, end-users can easily understand the Land Cover Classification System (LCCS (Di Gregorio, 2005)) entirely based on inference rules (e.g. a vegetated area covered by trees whose leaf type is"broadleaved" and leaf phenology is"evergreen" will be assigned to a land cover class named"broadleaved evergreen trees") but they can hardly interpret a classification model of the same class produced by a random forest or a deep learning classifier. Thus, such algorithms do not match with the way end-users are used to work.

As a consequence, users often consider data-driven approaches as"black box" algorithms whose use is not sufficiently documented in land cover mapping methods (Congalton et al., 2014). As a partial answer, recent efforts have been carried out to share methods and algorithms (instead of sharing ready-to-use maps) designed for remote sensing-based land surface monitoring (e.g. the CLASLite software (Asner, 2009), the EODHaM system (Lucas et al., 2015), the *iota2* processing chain (Inglada et al., 2017)). The application of such algorithms benefits from the emergence of online platforms dedicated to the cloud computing of large-scale geospatial data which allow both the production of high resolution maps and the sharing of image processing algorithms (Gorelick et al., 2017). By improving the transparency and democratization of high-performance technologies, such approaches contribute to facilitate the processing of big Earth Observation (EO) datasets by scientists from varied scientific domains, i.e. not only remote sensing experts. However, at the same time it fosters the use of EO data by non remote sensing experts, it also -and rather paradoxically- supports the evolution of remote sensing from an environmental science to a computer science with a major focus on image and signal processing (e.g. improved classification algorithms, analysis of big EO data time series, etc) rather than on the applications. The expert knowledge mobilized by environmental scientists to interpret remote sensing images thus tends to be somehow discarded from the image analysis.

Table 1
Definitions of main terms used in the paper.

Term	Definition
Ontology	Formal, explicit specification of a shared conceptualization (Gruber, 1993)
Geographic Feature	Abstraction of a real-world geographic phenomenon
Geographic Entity	Real-world entity that occupies a position in space (Mark, 1993)
Geographic Object	Digital representation of a geographic entity (Mark, 1993)
Intentionality	Purposes, intentions, motivations, needs, beliefs of an end-user (Couclelis, 1992)
Minor Entity	Immaterial entity (surfaces, shadows and holes) (Casati, 2009)
Observables	Properties that depend on perceptual experiences, e.g. colour and texture whose description is subjective and difficult to express (Couclelis, 2010)
Similarities	Properties that refer to measurable and objective characteristics, e.g. vegetation height (Couclelis, 2010)
OBOE	Formal ontology for capturing the semantics of scientific observation and measurement (Madin et al., 2007)
Knowledge-driven	Methods that depend on a priori knowledge, i.e the classification model exists regardless of the data
Data-driven	Methods that depend on the data, i.e the classification model does not exist if there is no data
EUEK	End-User Expert Knowledge, usually implicit, symbolic and vague
RSEK	Remote Sensing Expert Knowledge, usually numeric and implicit

To summarize, the continuous development of new sensors and easier access to remote sensing data (Sudmanns et al., 2019; Zhu et al., 2019) and techniques is transforming both the theory and practice of remote sensing (Arvor et al., 2019). The production of large-scale land cover maps is essential for many applications but the classification schemes and the methodological approaches present important limitations that may deepen the gap between the map producers and the end-users. In this context, the objective of this paper is to introduce a novel knowledge-driven methodological approach to automatically provide symbolic descriptions of time series of Sentinel-2 spectral signatures. These descriptions are based on low-level characteristics in order to avoid hasty over-interpretation with high-level semantic classes and thus reduce the sensory and semantic gaps. Then, the low-level descriptions can be adapted by the end-users to match their requirements. Section 2 presents the conceptual framework underlying our approach. Section 3 and Section 4 illustrate the implementation of the system through a concrete application in the Brazilian state of Mato Grosso. Section 5 discusses future perspectives to improve both the conceptual framework and the system's implementation.

2. Conceptual framework

In order to address the issues raised in the introduction section, we propose a knowledge-based approach that draws on a conceptual framework inspired from ontological modelling. The Table 1 defines the main terms used in the presentation of the conceptual framework.

2.1. Ontologies for the description of scientific observations

We rely on a conceptual model that allows describing the way experts observe geographic features of interest in remote sensing images. To do so, we inspired from ontologies especially designed to enable semantic and symbolic descriptions of scientific observations, such as

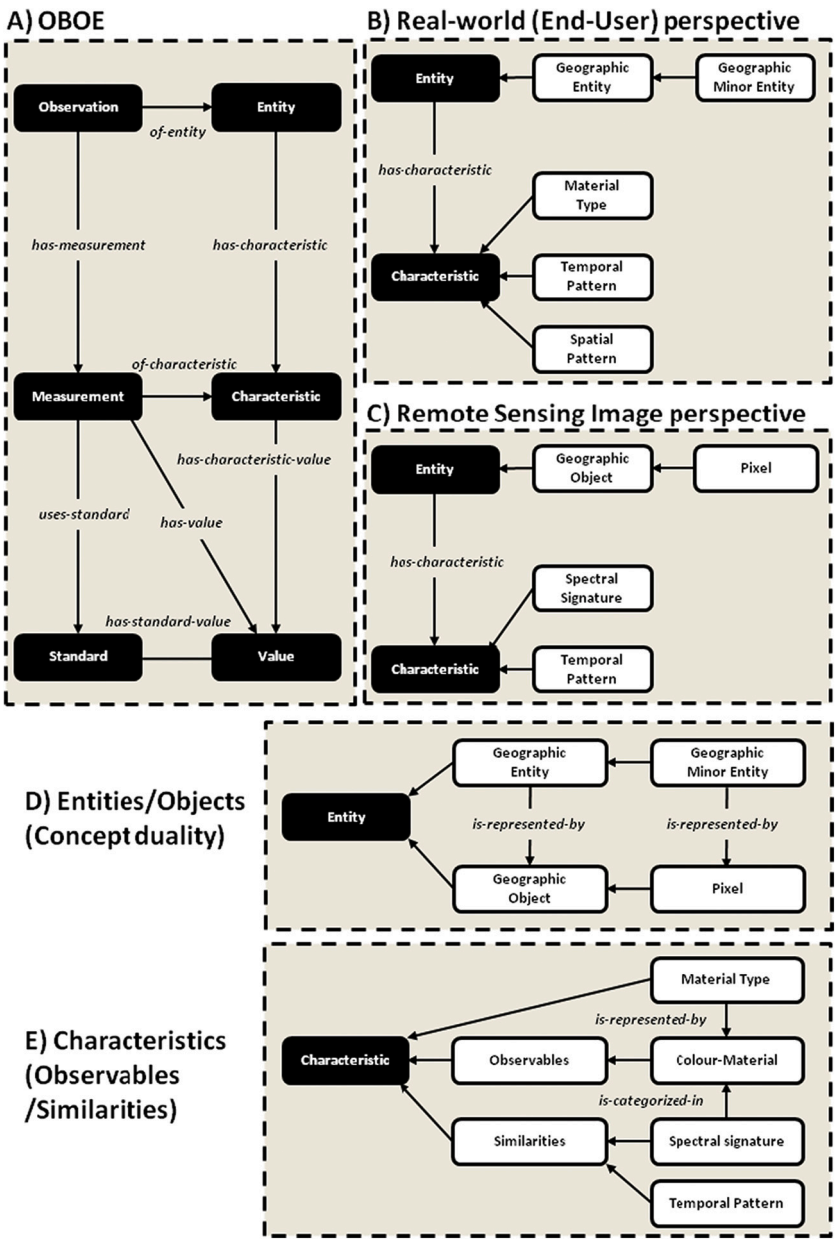

Fig. 1. Description of the ontological conceptual framework including (A) the Extensible Observation Ontology (OBOE), its application for the description of (B) geographic entities and (C) geographic objects, and its extension through the *Entity* (D) and *Characteristic* (E) concept.

Table 2
Steps of the semantic contraction proposed by Couclelis (Couclelis, 2010) and an example of its application (see also Section 3). Shaded rows identify the steps addressed in the present study.

Semantic resolution level	Example: A map of Permanent Protected Areas in Mato Grosso, Southern Brazilian Amazon
7 Purpose	Identify Permanent Protected Areas to be restored
6 Function	Represent the areas where natural vegetation has been degraded
5 Composite objects	A network of patches of natural vegetation
4 Simple Objects	Patches of natural vegetation
3 Similarities	Fields of measurable properties exhibiting diverse geometrical patterns (e.g. occurrences)
2 Observables	Field-like properties (e.g. Colours)
1 Existence	The relevant information exists at given spectral, spatial and temporal resolution

the Observation and Measurement (O&M) ontology (Cox, 2013) and the Extensible Observation Ontology (OBOE) (Madin et al., 2007; Madin et al., 2008). Both ontologies share many common concepts and can thus be aligned together. Here, we considered the OBOE ontology that provides a formal conceptual framework for capturing the semantics of scientific observations and measurements (Madin et al., 2007). To make it short, OBOE asserts that an *Observation* of an *Entity* is carried out through the *Measurement* of one (or more) *Characteristic* using a measurement *Standard*. Finally, the *Measurement* has a *Value*, which can either be numeric (e.g. a reflectance value) or literal (e.g. a class label) (Fig. 1A).

The OBOE ontology is called"extensible" because key concepts such as *Entity*, *Characteristic* or *Value* can be extended to include sub-concepts from a specific domain such as Earth Observation. For example, the *Forest* concept can be defined as a sub-class of *Entity*, *Leaf phenology* as a

sub-class of *Characteristic* and *Evergreen* as a sub-class of *Value*. In the following section, we better detail how we extended the concepts of *Entity* and *Characteristic* based on ontologies of geographic information. The extension of the *Value* concept is then further described in the application section.

2.2. Ontologies of geographic information

An efficient use of OBOE framework requires investigating the roles of language and cognition in humans' conceptualization of geographic concepts (Claramunt, 2020). Couclelis (Couclelis, 2010) introduced an ontological system to describe the observation of geographic features. This system is based on principles of cognitive geography, which is about the way humans understand, categorize and act in the geographic world (Couclelis, 1992). It takes the form of a suitably ordered *semantic contraction* made of seven levels differentiated by their degree of complexity, from highest (level 7) to lowest (level 1) (Table 2). According to Lang et al. (Lang et al., 2014),"the *semantic contraction* is a kind of backtracking concept from rich geospatial information that, stepwise, loses purpose, function, composition, and ultimately its space–time relations, down to a piece of information without spatial or temporal context." In this study, we focus on levels 1–3 of the semantic contraction corresponding to the field representation of geographic entities (pixel-based), in opposition to object representation at levels 4 to 7.

2.2.1. Purpose and existence

The main peculiarity of this hierarchy is that any geographic information is understood as a function of at least two kinds of separate considerations: purpose (intentionality) and existence (scale) (Couclelis, 1992). These two considerations (intention and scale) represent the two ends of the *semantic contraction*, i.e. level 7 and level 1 respectively. Intentionality refers to the purposes, intentions, motivations, needs, beliefs, and so on, of an observer or a user of the system (Couclelis, 2010). For example, an ecologist may consider a hedgerow separating two neighboring cultivated fields as a corridor that allows forest species to move in an agricultural landscape, whereas an agronomist may consider the same hedgerow as an obstacle that impedes disease dispersion between two crop fields. These different point-of-views will drive the intentions of these two scientists at the time of mapping hedgerows, and consequently impact on their mapping requirements. The ecologist may require hedgerows to be represented as superficial areas to focus on their characteristics (e.g. width, internal heterogeneity) while the agronomist may represent them as lines.

In consequence, the intention of the end-users impacts the scale of analysis, which consists in identifying an appropriate spatio-temporal framework that enables to observe an entity (Couclelis, 2010). It thus refers to the existence of the entity at a particular granule of space and time. It is then an issue to determine the geographic features that can be observed in the data to be processed, e.g. 10 m resolution Sentinel-2 images at a 5–10 days temporal resolution. With regards to the temporal resolution, a critical issue to consider is: does a given remote-sensing tool describe change over time in a manner consistent with the ongoing process of interest (e.g. ecological processes, deforestation, urbanization)? (Kennedy et al., 2014). For example, information on vegetation phenology does not exist in single date remote sensing images and requires a multitemporal analysis. Similarly, considering that the spatial resolution of a sensor system should be less than half the size of the feature measured in its smallest dimension (Jensen, 1983), it gives an indication about the kind of geographic features that can (e.g. fields, forests, urban areas, large farm dams, etc) or cannot (e.g. plant crops, individual trees, houses, swimming pools, etc) be observed in 10 m resolution remote sensing images. In other words, we consider that, at this resolution, it is appropriate to map geographic spaces as defined by Freundschuh and Egenhofer (Freundschuh and Egenhofer, 1997), i.e. very large, non-manipulable spaces that due to practical limitations cannot be experienced via locomotion (e.g. agricultural landscapes, urban areas).

2.2.2. Entities

Between these two extremities (i.e. purpose and existence), the levels 4–7 of the semantic contraction are focused on the description of geographic entities. It is worth noting that these levels can be collapsed as the semantics of the system contracts (Couclelis, 2010). For example, a label of"Forest" can be assigned to a simple object (Level 4), carrying implicit information about its function (Level 6) and purpose (Level 7) according to a given user.

The *Entity* concept of the OBOE ontology was then extended to introduce the *Geographic Entities* of interest for the end users (Fig. 1B). A *Geographic Entity* is a real-world entity that occupies a position in space (e.g. a forest, a building), i.e."for every set of coordinates in space, there is corresponding to it or associated with it, an instance of one or more substance terms" (Sack, 2010). In philosophy, material substances are hylomorphic compounds that can be described by their form and matter. In other words, a *Geographic Entity* can be characterized by the type of material of which it is composed (e.g. vegetation) and its associated form, i.e. its spatial (e.g. geometry) and/or temporal (e.g. phenology) pattern.

In addition, it is worth noting that real-world material entities (e.g. geographic entities) refer to major entities that should be differentiated from minor entities, i.e. immaterial entities (Casati, 2009). Minor entities are dependent entities since their existence depends on major entities. Minor entities are surfaces, shadows and holes, where holes are defined as negative entities, i.e. local privations of matter. When applied to the case of remote sensing image classification, optical satellite images can only be used to observe *Geographic Minor Entities*, i.e. land surfaces, shadows and clouds, the latter being assimilated to holes since they hinder the visualization of land surfaces (Fig. 1B).

On the other hand, since we are interested in interpreting remote sensing images, we do not actually intend to classify *Geographic Entities* but rather their representation in satellite images. For this reason, we need to consider the concept duality issue between *Geographic Entities* and *Geographic Objects* (Arvor et al., 2019) (Fig. 1D). An object is an *Entity* in the digital world, which represents real-world phenomena as an instance of a generally recognized category (Voudouris, 2010). A *Geographic Object* is then defined as a bounded geographic region in the digital world that can be identified for a period of time as the referent of a geographic term (Castilla and Hay, 2020). It is noteworthy that, although both geographic entities and corresponding objects are naturally correlated, there is no semantic identity between them since both cannot be described with the same characteristics from the ground and from satellite images. Whereas a *Geographic Entity* (e.g. a forested area) can be characterized by its matter (e.g. vegetation) and form, i.e. its spatial (e.g. patch size) and temporal pattern (e.g. leaf phenology), its representation in an image may be described by its pixel characteristics, i.e. spectral, spatial (e.g. texture) and temporal pattern (e.g. time series analysis) (Fig. 1C). This brings us to extend the *Characteristics* concept of the OBOE ontology.

2.2.3. Characteristics: observables and similarities

The 2nd (Observables) and 3rd (Similarities) levels of the semantic contraction are centered on the measurement of characteristics enabling the identification of geographic features. These characteristics refer to field properties, i.e. spatially connected areas that share common characteristics (Fig. 1E).

Similarities are measurable and objective field properties of geographic features (e.g. vegetation height, leaf type, etc) (Couclelis, 2010). Such characteristics can be associated to categorical (e.g."Broadleaved") or numeric (e.g."20 m") values. In remote sensing, such *Similarities* may stand for spatial (e.g. area of a field of pixels sharing common characteristics) and temporal characteristics (e.g. occurrence of a given class in a time series). But, in the case of a pixel-

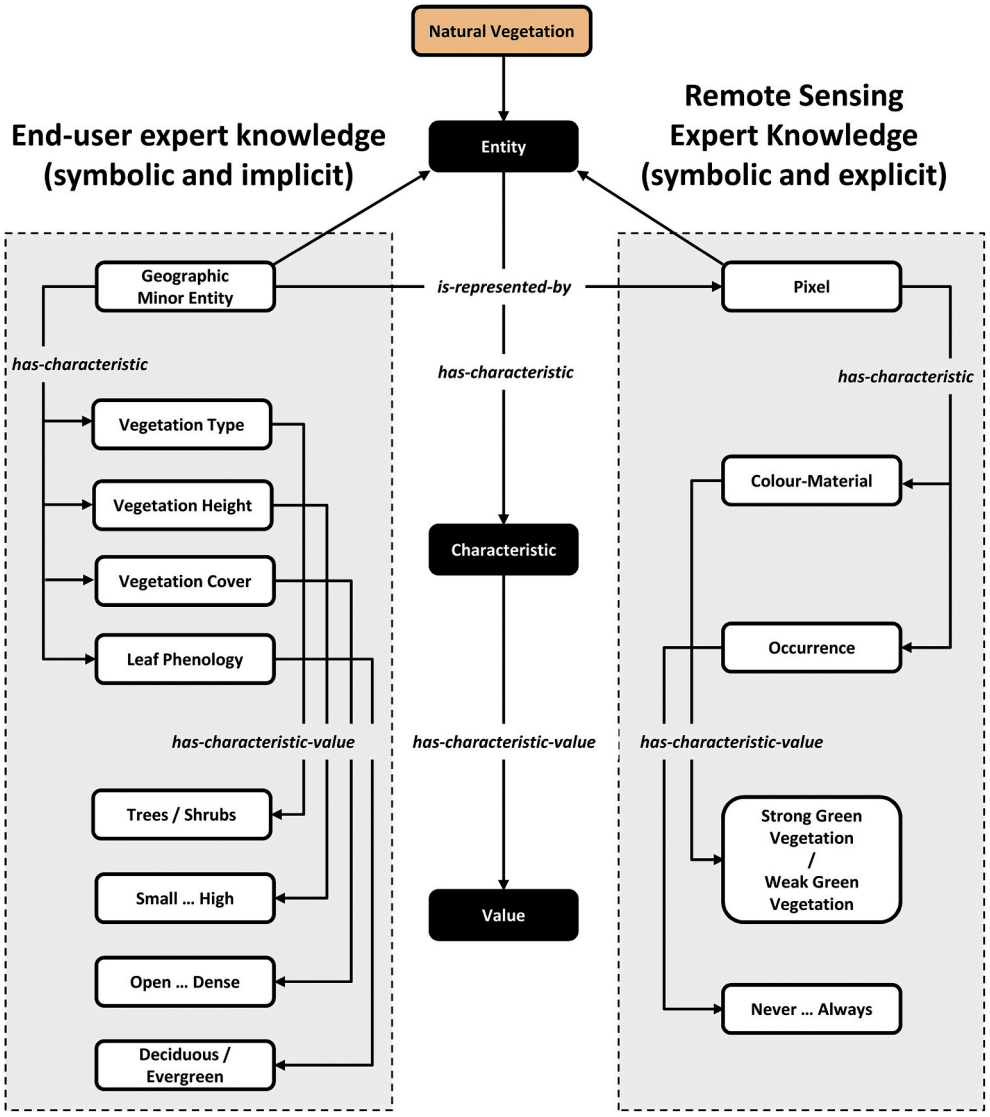

Fig. 2. Application of the ontological conceptual framework to describe the"Natural Vegetation" concept and its representation in a remote sensing image.

based classification, the geometrical shape is determined by the pixel's shape (i.e. approximated to a square) and thus cannot be considered to qualify a material type. Consequently, in agreement with the"time-first, space-later" approach (Camara et al., 2016; Picoli et al., 2018), we focused on temporal *Similarities*.

The spectral signature can also be considered as a *Similarities* characteristic since it is made of objective numeric reflectance values. However, its classification into spectral categories is subjective and open to debate, depending on the operator's experience and intentions. In that sense, unlike reflectance values that refer to Similarities, spectral categories can be considered as *Observable* characteristics, which refer to Sense Qualia properties, i.e."certain features of the bodily sensations especially, but also of certain perceptual experiences, which no amount of purely physical information includes" (Jackson, 1982). *Observables* are field-like properties that cannot be measured (Couclelis, 2010). Colour is a typical *Sense Qualia* whose perception is subjective and difficult to communicate. For example, the perception of shades of green to describe vegetated surfaces vary among humans (e.g."green like a rain forest" or"green like a lemon"). According to Jensen (Jensen, 1983), *Colour and the spectral signature* is a fundamental biophysical variable amenable to remote sensing. More specifically, remote sensors measure"spectral signatures of the material within a pixel, thus gaining insight about an object's colour in the visible spectrum and also document its reflectivity beyond our human experience". In other words, classifying spectral signatures means classifying colours of land surface material types. For this reason, we categorized spectral signatures including spectral bands from the non-visible spectrum in classes of *Colour-Material*, which is then an *Observable* characteristic related to a land surface material type (Fig. 1E).

2.3. End-user expert knowledge vs remote sensing expert knowledge

Once the ontological framework has been defined, further clarifications on the expert knowledge to be described are necessary. Although the end-users are often the map producers themselves, we here differentiate the end-user expert knowledge (EUEK) from the remote sensing expert knowledge (RSEK) (Fig. 2). EUEK refers to the description of a geographic feature of interest from a real-world perspective whereas RSEK refers to the description of its representation from an image perspective. EUEK is often symbolic, implicit and vague. For example, while defining a"Natural Vegetation" land cover class,"one must recognize that there are often several communities that could be the"-natural" vegetation for any given site at any given time" (Sprugel, 1991). That being said, one may assume that"Natural Vegetation" includes a vegetation gradient that could be described (although the definition remains implicit) by physical characteristics (and their corresponding

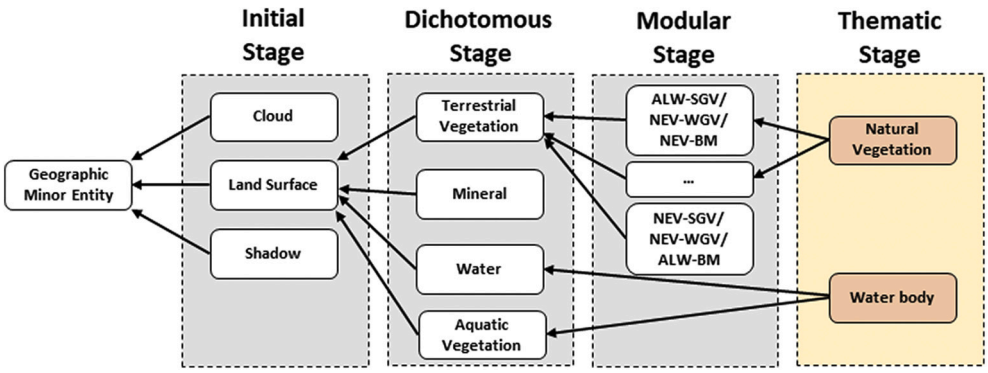

Fig. 3. Classes of *Geographic Minor Entities* mapped at each stage of the classification system.

values) such as vegetation type (Trees, Shrubs, etc.), vegetation height (small to high), vegetation cover (open to dense) or leaf phenology (evergreen or deciduous).

On the other hand, RSEK is numeric (in opposition to symbolic) and implicit, especially when expressed in hardly interpretable classification models. In this regard, reducing the gap between EUEK and RSEK appears challenging. Since explicitly defining vague and ambiguous concepts of the EUEK may be unrealistic (Sprugel, 1991), we consider that the priority is to formalize the implicit and numeric RSEK into an explicit and symbolic knowledge (Fig. 2). To do so, we need to define the image characteristics (and their corresponding values) to formalize RSEK. This is a major objective of the system introduced in this paper.

2.4. System's architecture

Based on these findings, we implemented a classification system

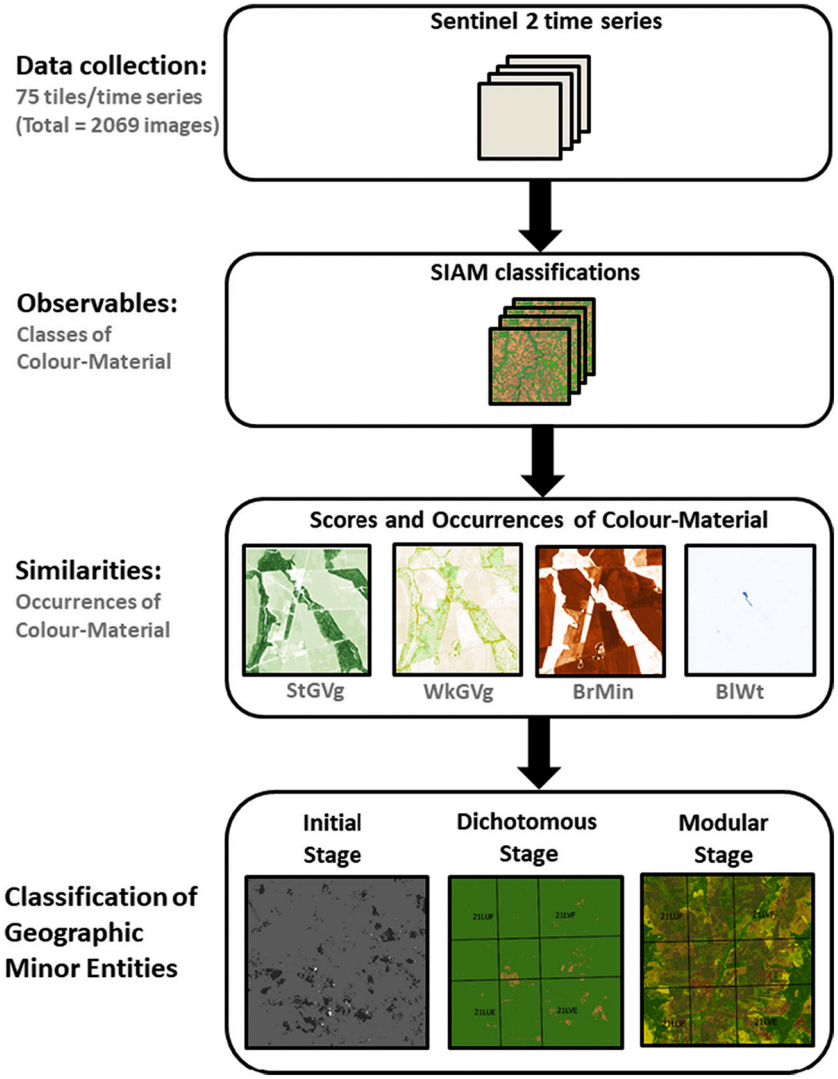

Fig. 4. Flowchart of the proposed methodology to process Sentinel-2 time series.

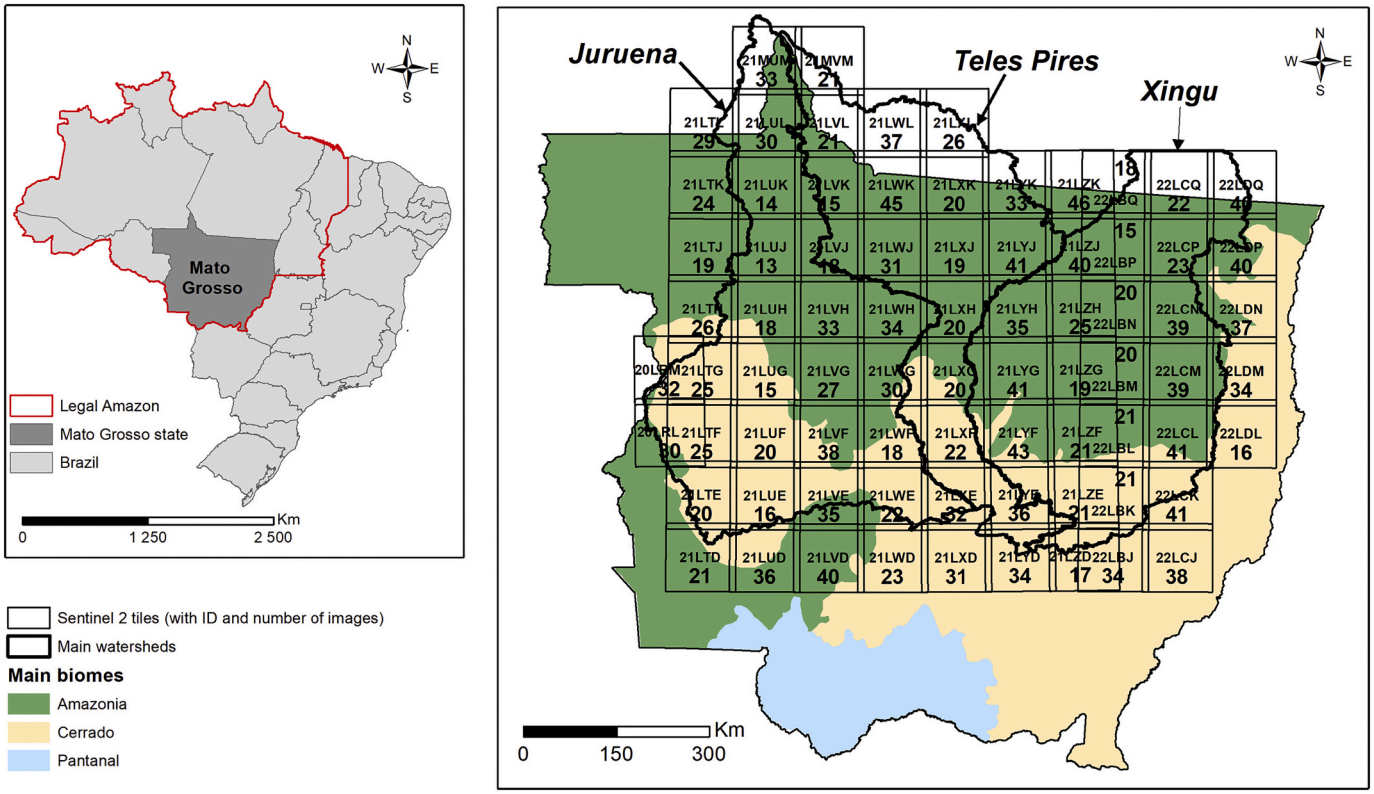

Fig. 5. Location of the study area and identification of the Sentinel-2 tiles and their corresponding number of images.

inspired from the LCCS but focused on the description of image characteristics (instead of real-world characteristics in LCCS) defined to describe *Pixels* and relate them to *Geographic Minor Entities* of interest for the end-user. The system is divided in four successive stages (Fig. 3):

- **Initial stage**: to discriminate land surfaces, clouds and shadows.
- **Dichotomous stage**: to discriminate land surface material types, e.g. vegetated, mineral and aquatic areas.
- **Modular stage**: to refine the description of land surface material types with additional characteristics in order to provide more complex low-level symbolic descriptions.
- **Thematic stage**: to allow the end-users to relate the modular classes with high-level semantic labels, e.g. natural vegetation and water bodies.

At each stage, the ontological conceptual framework is primarily used to explicit the information contained in the time series of spectral signatures of every pixels, while the end-user conceptualization of a *Geographic Minor Entity* can remain implicit (Fig. 2). The system is thus primarily designed to describe the information available in the remote sensing images, rather than to describe real-world entities, which is in line with the original approach proposed by (Couclelis, 2010)"whereby it is the information available about the world, and not the world itself, that forms the basis of the ontological system". The explicit descriptions of pixels are built using symbolic natural language assertions in order to ease the interpretability of the classification rules by the end-users (Assertion 1). By doing so, we intend to reduce the semantic and sensory gaps, allowing the end-user freedom to do the final relation between the geographic entity of interest (e.g. *Natural Vegetation*) and the pixel's description.

Assertion 1. *A ["Geographic Object"] represents a ["Geographic Minor Entity"] if that ["Geographic Object"] is [a value to qualify an Occurrence characteristics] classified as [a value to qualify a Colour-Material characteristic].*

For example, a"pixel" represents a"Natural Vegetation" if that"pixel" is"always" classified as"Strong Green Vegetation".

3. Application

Based on this conceptual framework, we implemented an automatic knowledge-driven approach to classify Sentinel-2 time series in the Southern Brazilian Amazon. This approach is summarized in Fig. 4.

3.1. Intention and scale: end-users, study area and data

In order to test our approach, we worked in close cooperation with the *Instituto Centro de Vida* (ICV), a Brazilian Non-Governmental Organization (NGO) acting for environmental preservation in the Southern Amazon. This NGO is very active in monitoring the application and efficiency of environmental public policies in the Amazon. For example, ICV aims at assessing the level of compliance of private rural properties with the environmental legislation, as defined in the Brazilian Forest Code (Stickler et al., 2013; Taniwaki et al., 2018) and required for the Rural Environmental Registry (CAR) (Roitman et al., 2018). As a major example, ICV has been mandated by the Mato Grosso State Secretary for Environment (SEMA-MT) to produce the 2008 map of consolidated rural areas (CRA) (Arvor et al., 2021). The concept of consolidated rural area is legally defined as the area of a rural property under human occupation (i.e. water bodies and urban areas are not considered as CRA) before the reference date of July 2008. This map is of particular importance since it serves as a basis for the implementation of the Environmental Regularization Program (PRA), which has suspended all sanctions for environmental infractions that occurred before July 22, 2008. Although the sole map of 2008 serves as a legal basis, it needs to be updated to detect potential illegal land use changes (i.e. deforestation). To do so, ICV relies on the laborious and time-consuming visual interpretation of very high resolution images (mainly SPOT-5 images at 2.5 m spatial resolution) to discriminate occupied rural areas from natural vegetation. In addition,

ICV leads important local and regional initiatives to support the restoration of Permanent Protected Areas (APP), i.e. riparian forests protected by law (Taniwaki et al., 2018). This implies 1) to map water bodies, especially small and large water dams designed for energy production, irrigation and fish farming and whose proliferation represents a major environmental concern (Souza et al., 2019; Arvor et al., 2018), and 2) to locate and quantify corresponding degraded riparian vegetation. For these reasons, we focused our study on two classes: 1) natural vegetation, with a special emphasis on riparian forests, and 2) water bodies, with a special emphasis on small water bodies. Finally, it is worth noting that, although the end-user is a GIS team from ICV with a long expertise in remote sensing, all the image processing tasks introduced in that paper have been computed by the research team.

The study area is located in the Southern Amazon Brazilian state of Mato Grosso (Fig. 5) and covers three Amazonian watersheds (529.780 km^2), i.e. the Juruena (197.036 km^2), Teles Pires (144.955 km^2) and Xingu (187.789 km^2) watersheds. Only the part of the basins located in the state of Mato Grosso were considered. This region is of special interest for two main reasons. First, it includes a south-north gradient of natural vegetation ranging from Brazilian savannas (*Cerrado*) to dense evergreen rainforests. Second, despite the delineation of many protected areas (e.g. the Xingu indigenous land), it has suffered from intense land cover changes during the last four decades. Indeed, a rapid colonization process initiated in the 1970s has been supported by the government to promote agricultural development. As a consequence, major land use types encountered in the Amazon are represented in the study area, i.e. small- and large-scale agriculture, pasture, reforestation, degraded forests, timber logging, urban areas, natural and artificial water bodies. This diversity of natural and anthropogenic land cover/use types draws scholars' attention from diverse scientific areas (e.g. geography, agronomy, hydrology, climatology, ecology) and turns automatic land cover mapping a challenging task.

In order to map this study area, we downloaded Sentinel-2 images for the year 2017 and spread across 75 tiles covering a total area of 726,981 km^2. Although we requested images with a low cloud cover rate (below 50%), we noticed through visual inspection that many images still presented much higher cloud cover rates. For this reason, we manually discarded unusable data and finally acquired a total of 2069 Level 1-C Sentinel-2 images, i.e. 1793 Sentinel-2A images and 276 Sentinel-2B images. The entire dataset thus consisted in 75 time series including from 13 to 46 images. We used Top-of-Atmosphere reflectances of six spectral bands (R, G, B, NIR, SWIR1, SWIR2) in order to apply the Satellite Image Automatic Mapper (SIAM) algorithm (see Section 3.2.1). All bands were resampled at 10 m spatial resolution with a bilinear algorithm in order to benefit from the highest spatial resolution.

3.2. Image processing: characteristics

We first processed the Sentinel-2 time series to compute the *Observables* and *Similarities* characteristics as explained in Section 2.2.3. In this application section, we put a special emphasis on the methods and *Values* (or labels) chosen to describe these *Characteristics*.

3.2.1. Observables: classes of colour-material

Since *Observables* refer to *Sense Qualia* field-like properties, the major issue consists in assigning meaningful labels (i.e. values) to describe them, especially to describe spectral signatures. In this regard, models of qualitative colour description (e.g. (Falomir et al., 2013)) include colour labels (e.g."pale-blue","light-green") that appear limited to define remotely sensed spectral signatures including reflectances in spectral bands not accessible for human vision. The objective is then to define rules to categorize spectral signatures involving spectral bands from the non-visible spectrum, adding them semantic values corresponding to classes of *Colour-Material*.

We relied on the seminal work from Baraldi et al. (Baraldi et al., 2006) to process all images of the database. The Satellite Image Automatic Mapper (SIAM) is a rule-based per pixel classifier based on spectral-domain prior expert knowledge taken from the remote sensing literature (Baraldi et al., 2006). It thus does not require any training data and can be considered as a knowledge-driven approach (in opposition to a data-driven approach as explained in Section 1.2) relying on remote sensing expert knowledge. SIAM assigns pixels to spectral categories exclusively based on relative rules (i.e. applied on spectral indices and on ratios between spectral bands). As such, it aims at describing the pattern of the spectral signature rather than its absolute spectral values and can thus be applied to top-of-atmosphere or surface reflectance values. Finally, the resulting spectral categories do not correspond to land cover classes but should rather be considered as labels describing spectral signatures. For example, the *SVHNIR* spectral category refers to *Strong Vegetation with High Near-Infrared* values.

All SIAM spectral rules are introduced in (Baraldi et al., 2006) and

Table 3
List of SIAM spectral categories for Sentinel-2 with associated classes of *colour-material*.

ID	Label	Spectral category	Colour	Colour-material
1	CL	Cloud		White Cloud
2	SN	Snow		
4	ICSN	Ice or Snow		
5	DPWASH	Deep Water or Shadow		Blue Water
6	SLWASH	Shallow Water or Shadow		
7	PBHNDVI	Pit bog with High NDVI		Weak Green Veg.
8	PBMNDVI	Pit bog with Medium NDVI		
9	PBLNDVI	Pit bog with Low NDVI		
10	SVHNIR	Strong Vegetation with High NIR		Strong Green Veg.
11	SVLNIR	Strong Vegetation with Low NIR		
12	AVHNIR	Average Vegetation with High NIR		
13	AVLNIR	Average Vegetation with Low NIR		
14	WVHNIR	Weak Vegetation with High NIR		Weak Green Veg.
15	WVLNIR	Weak Vegetation with Low NIR		
16	SSRHNIR	Strong Shrub Rangeland with High NIR		
17	SSRLNIR	Strong Shrub Rangeland with Low NIR		
18	ASRHNIR	Average Shrub Rangeland with High NIR		
19	ASRLNIR	Average Shrub Rangeland with Low NIR		
20	SHR	Strong Herbaceous		
21	AHR	Average Herbaceous		
22	DR	Dark Rangeland		
23	BBBHNDBBBI	Bright Barren Land with High NDBBBI		White Cloud
24	BBBLNDBBBI	Bright Barren Land with Low NDBBBI		Brown Mineral
27	SBBF	Strong Barren Land with flat response		
28	SBBNF	Strong Barren Land with non-flat response		
31	ABBHNDBBBI	Average Barren Land with High NDBBBI		
32	ABBLNDBBBI	Average Barren Land with Low NDBBBI		
35	DBBF	Dark Barren Land with flat response		
36	DBBNF	Dark Barren Land with non-flat response		
39	WR	Weak Rangeland		White Cloud
40	SHV	Shadow area with vegetation		Black Shadow
41	SHB	Shadow area with barren land		
42	SHCL	Shadow clouds		
43	TWASHSN	Shadow snow		
44	WE	Wetland		
45	TWA	Turbid Water		Blue Water

thus not repeated here. Nonetheless, it is worth noting that, since the method has initially been designed for Landsat-5 (TM) and Landsat-7 (ETM+) images, a few adaptations were required in order to be applied to other optical sensors (Baraldi et al., 2010). For example, the absence of the thermal band in Sentinel-2 images needed to be addressed since it is used to discriminate a few spectral categories. In that case, all spectral categories whose corresponding rule set implied the thermal band were removed so that the final Sentinel-2 pre-classifications only considered up to 36 spectral categories whereas the original SIAM version implemented for Landsat data can identify up to 46 spectral categories. Also, it is worth noting that the red-edge band of Sentinel-2 images was not used in this study since the original version of SIAM designed for Landsat data did not include any rule for this specific band.

In addition, the spectral categories corresponding to cloud classes are based on the thermal band and could not be applied to Sentinel-2. Since cloud masking is very important, we created an equivalent spectral category in order to map clouds. For this purpose, we first intended to use the cloud mask product released with Level 1-C Sentinel-2 data. However, this product has been considered as highly inefficient in Amazonian rainforests due to the presence of complex cloudiness and high water vapor content (Coluzzi et al., 2018). Various software and algorithms to map clouds (and cloud-shadows) in Sentinel-2 images were then proposed recently (Frantz et al., 2018; Zhu et al., 2015). In this study, we implemented a ready-to-use decision tree designed to map clouds in order to be coherent with the overall approach based on decision rules. This decision tree has been proposed by Hollstein et al. (Hollstein et al., 2016) and the spectral rules for cloud masking are defined in Eq. (1):

$$
\begin{aligned}
&Cloud = \\
&\left[(B_3 < 0.139) \quad AND \quad (B_{8A} < 0.166) \quad AND \quad \left(\frac{B_2}{B_{10}} < 16.689\right) \quad AND \quad \left(\frac{B_2}{B_9} \geq 0.788\right)\right] \\
&\text{OR} \\
&\left[(B_3 \geq 0.139) \quad AND \quad \left(\frac{B_5}{B_{11}} < 4.33\right) \quad AND \quad (B_{11} - B_{10} < 0.255)\right] \\
&\text{OR} \\
&\left[(B_3 \geq 0.139) \quad AND \quad \left(\frac{B_5}{B_{11}} < 4.33\right) \quad AND \quad (B_{11} - B_{10} \geq 0.255) \quad AND \quad (B_1 \geq 0.3)\right]
\end{aligned}
\tag{1}
$$

where B_i refers to the i^{th} Sentinel-2 spectral band.

At the end, the pre-classifications consisted in 36 spectral categories listed in Table 3. The labels assigned to SIAM spectral categories can be considered as related to the surface material type being observed at a given date. For example, the *BBBHNDBBBI* label refers to a spectral category that qualifies the spectral signature of a bright barren land. Nonetheless, it does not necessarily means that all pixels assigned to this label represent bright barren lands due to confusions that may exist with other classes with close spectral signatures. For example, we noticed that the *BBBHNDBBBI* and the *WR* (Weak Rangeland) categories often corresponded to clouds. Thus, in order to limit confusions between categories and simplify the analysis, the SIAM spectral categories were reclassified in six main classes of *colour-material*, whose labels were constructed by associating a colour with the most likely corresponding geographic minor entity (i.e. land surface material type, clouds and shadows). The six classes of *colour-material* were:"White Cloud" (WhCl),"Black Shadow" (BlSh),"Blue Water" (BlWt),"Strong Green Vegetation" (StGVg),"Weak Green Vegetation" (WkGVg) and"Brown Mineral" (BrMin). The"White Cloud" label then refers to a field-like property, i.e. it describes a pixel whose spectral signature looks like a cloud spectral signature, but not necessarily representing a cloud due to potential confusions (with buildings for example, see Supplementary Material 5). The correspondences between the original SIAM spectral categories and the *colour-material* classes are defined in Table 3.

3.2.2. Similarities: descriptors of time series

Similarities refer to objective and measurable characteristics. Here, we emphasized the importance of the temporal characteristics to describe land surface material types. In this regard, we implemented a scoring approach computed on a per-pixel basis which simply consists in counting (i.e. summing) the occurrences of a *colour-material* class in a time series. At each date, the counting is weighted by the quality of the corresponding image considering its cloud cover rate. For example, a pixel assigned to the *SVHNIR* spectral category in an image with a 30% cloud cover was attributed a score of 0.7 (70%) to the corresponding"Strong Green Vegetation" *colour-material* class. By doing so, the objective was to give more importance to pixels observed in high quality cloud-free images while the information contained in pixels observed in low quality images was more uncertain. Finally, each pixel time series is described by six scores corresponding to the six classes of *colour-material*. These scores were then used to derive various information.

First, the"Best Possible Score" (BPS) corresponds to the sum of all six scores. It represents the maximum score potentially assigned to a pixel that would always be classified in the same class of *colour-material*. BPS gives a first broad overview of pixel quality since it is related to the number of observations, thus considering the inhomogeneity of the data (Sudmanns et al., 2019).

$$Score_{BPS} = \sum Score_{colour-material} \tag{2}$$

where $Score_{colour-material}$ refers to the scores of the six classes of *colour-material*.

Second, the"Best Land Surface Score" (BLSS) is the sum of all scores corresponding to classes of *colour-material* related to a land surface material type, i.e. all classes except"White Cloud" and"Black Shadow" (Eq. (3)). The BLSS ranges from 0 (when a pixel is never classified in any *colour-material* class related to a land surface material type) to the BPS value of the corresponding time series (when a pixel is always classified in the same *colour-material* class). In this regard, it can be considered as an indicator of pixel quality, with higher values corresponding to higher-frequency observations, and consequently better descriptions of the land surface material types.

$$Score_{BLSS} = Score_{BPS} - (Score_{WhCl} + Score_{BlSh}) \tag{3}$$

where $Score_{WhCl}$ and $Score_{WlSh}$ refer to the scores of the"White Cloud" and"Black Shadow" classes of *colour-material*, respectively.

Third, we calculated the ratio between the scores of *colour-material* classes related to land surface material types and the BLSS in order to compute the occurrence of each *colour-material* class, i.e. the proportion (in %) of observations in a given *colour-material* in a time series (Eq. (4)). These occurrences were then partitioned in eight categories labeled with

Table 4
Temporal rules to define temporal occurrences. $OCC_{colour-material}$ refers to the occurrence of each class of *colour-material*.

Adverb of time	Logical rule	Label	ID
Never	$Score_{colour-material} <= 1$	NEV	1
Rarely	$0\ \% \leq OCC_{colour-material} < 10\%$	RAR	2
Sometimes	$10\ \% \leq OCC_{colour-material} < 25\%$	SOM	3
Regularly	$25\ \% \leq OCC_{colour-material} < 50\%$	REG	4
Predominantly	$50\ \% \leq OCC_{colour-material} < 75\%$	PRED	5
Usually	$75\ \% \leq OCC_{colour-material} < 90\%$	USU	6
Often	$90\ \% \leq OCC_{colour-material} < 99\%$	OFT	7
Always	$OCC_{colour-material} >= 99\%$	ALW	8

adverbs of time to remain as close as possible to natural language. These adverbs were:"Never","Rarely","Sometimes", "Regularly","Predominantly","Usually","Often" and"Always". The thresholds adopted to define each adverb are listed in Table 4. It is worth mentioning that the"Never" adverb is chosen when a score is $<= 1$ in a given *Colour-Material* class in order to avoid giving too much importance to pixels with low absolute score values but high occurrence values.

$$OCC_{colour-material} = \frac{Score_{colour-material}}{Score_{BLSS}} \tag{4}$$

where $OCC_{colour-material}$ stands for the occurrence (in %) of values for a given class of *colour-material*.

3.3. Classification of geographic minor entities

3.3.1. Initial stage

At this level, the objective is to discriminate land surfaces, clouds and shadows. For this purpose, we set the assertions 2 to 4 to explicitly describe these classes in natural language.

Assertion 2. *A pixel represents a land surface if that pixel is (at least) sometimes classified in a Colour-Material class that refers to a land surface,* i.e.*"Blue Water" or"Brown Mineral" or"Strong Green Vegetation" or"Weak Green Vegetation".*

Assertion 3. *A pixel represents a cloudy area if that pixel is not classified as land surface but (at least) often classified as either"White Cloud" or"Brown Mineral" Colour-Material.*

Assertion 4. *A pixel represents a shadow area if that pixel is neither classified as land surface nor cloudy area.*

These assertions are expressed in Eq. (5):

$$MinorEntity = \begin{cases} LandSurface, & \text{if } (OCC_{BLSS} >= 10\%) \\ Cloud, & \text{if } (OCC_{WhCl+BrMin} \geq 90\%) \\ Shadow, & \text{Otherwise} \end{cases} \tag{5}$$

where OCC_{class} refers to the occurrence of the corresponding *class* of *Colour-Material*, i.e. *WhCl* and *BrMin* stand for"White Cloud" and"Brown Mineral", respectively.

3.3.2. Dichotomous stage

The dichotomous stage aims at discriminating land surface material types. It thus produces a broad classification to separate large chunks of matter considering vegetated and aquatic areas as proposed in the two first steps of the Land Cover Classification System (LCCS; (Di Gregorio, 2005)).

Firstly, we computed a binary*"Realm"* classification to differentiate"Aquatic" and"Terrestrial" areas. In this regard, the natural language description of a pixel belonging to the"Aquatic" class is expressed in assertion 5.

Assertion 5. *A pixel represents an aquatic area if that pixel is (at least) usually classified as"Blue Water" Colour-Material class.*

Table 5
Description, label, colour and ID of classes at dichotomous stage.

Description	Label	Colour	ID
Terrestrial Vegetation	Ter_Veg		10
Terrestrial Non-Vegetation	Mineral		20
Aquatic Vegetation	Aqu_Veg		30
Aquatic Non-Vegetation	Water		40
Clouds	Cloud		50
Shadows	Shadow		60

$$Realm = \begin{cases} Aquatic, & \text{if } (OCC_{BlWt} \geq 50\%) \\ Terrestrial, & \text{Otherwise} \end{cases} \tag{6}$$

where OCC_{BlWt} refers to the occurrence of the"Blue Water" *Colour-Material*.

Secondly, a binary*"Substance"* classification was computed to discriminate"Vegetation" and"Non-vegetation" areas. As expressed in assertion 6 and in Eq. (7), we classified a pixel as"Vegetation" if it is observed in"Green Vegetation" (either Strong or Weak Green Vegetation) at least once in a time series. Indeed, due to phenological cycles and agricultural calendars, pixels corresponding to vegetated areas are not always observed as vegetation. For example, in our case study, most cloud-free images are acquired during the dry season (July–August, (Asner, 2001; Sano et al., 2007; Martins et al., 2018)) when many fields are non-vegetated since crops are cultivated during the rainy season.

Assertion 6. *A pixel represents a vegetated area if that pixel is not never classified as"Strong Green Vegetation" or"Weak Green Vegetation" in a time series.*

$$Substance = \begin{cases} Vegetation, & \text{if } \left(Score_{StGVg+WkGVg}\right) > 1) \\ Non-Vegetation, & \text{otherwise} \end{cases} \tag{7}$$

where $Score_{SGVg+WGVg}$ refers to the sum of scores in"Strong Green Vegetation" and"Weak Green Vegetation", respectively.

Finally, these two binary classifications were crossed together to produce the dichotomous stage classification including the following four classes of land surface material types: Terrestrial Vegetation, Mineral (i.e. Terrestrial Non-Vegetation), Aquatic Vegetation and Water (i.e. Aquatic Non-Vegetation). In addition, Cloud and Shadow pixels identified at the initial stage are also preserved (Table 5).

3.3.3. Modular stage

At the modular stage, the descriptions of land surface material types observed at dichotomous stage were extended by associating additional *Similarities* characteristics, especially considering the occurrences of *Colour-material* classes. The objective was to assign each pixel to a label that explicitly describes its time series of spectral signatures.

In the present case, we only extended the"terrestrial vegetation" class identified at the dichotomous stage to add temporal characteristics. We focused on that class since the end-user (ICV) was mainly interested in mapping natural vegetation and water bodies, the latter being already identified at the dichotomous stage. Although it is worth reminding that the image characteristics (*Colour-material* and occurrences) are not direct measurements of real-world characteristics, we consider that 1) *colour-material* classes provide information on photosynthetic activity and vegetation structure (canopy structure or vegetation cover) in a given time whereas 2) occurrence of *colour-material* classes is related to vegetation phenology (see also Supplementary Material 1 to see comparisons of the final modular classification with vegetation cover products).

The terminology used at the modular stage was constructed by associating adverbs of time with classes of *colour-material*. All pixels were assigned a composite label describing the temporal signatures based on the possible combinations between the occurrences of"strong Green Vegetation","Weak Green Vegetation" and"Brown Mineral"

Table 6
Examples of IDs, labels, colours and potential associated land cover classes defined at the modular stage.

ID	Colour/Label	Vegetation Gradient
118	NEV-SGV/NEV-WGV/ALW-BM	Permanent Bare Soil (Urban)
136	NEV-SGV/SOM-WGV/USU-BM	
316	SOM-SGV/NEV-WGV/USU-BM	Crops
345	SOM-SGV/REG-WGV/PRED-BM	
163	NEV-SGV/USU-WGV/SOM-BM	Herbaceous Vegetation
181	NEV-SGV/ALW-WGV/NEV-BM	(Pasture, Open Cerrado)
361	SOM-SGV/USU-WGV/NEV-BM	
541	PRED-SGV/REG-WGV/NEV-BM	Woody Vegetation
631	USU-SGV/SOM-WGV/NEV-BM	
811	ALW-SGV/NEV-WGV/NEV-BM	Evergreen Forest

Colour-Material classes. The"Blue Water" class was not considered here since we were only focusing on areas of"Terrestrial Vegetation". An example of composite label is"ALW-SV & NEV-WV & NEV-BM", which refers to a pixel *always* classified in"Strong Green Vegetation" and *never* in"Weak Green Vegetation" nor"Brown Mineral". This approach leads to a maximum of $N = 512$ combinations, from which many of them are impossible. For example, a pixel cannot be *always* classified as Strong Green Vegetation and Weak Green Vegetation in the same time.

In addition, each composite label is associated to a 3-digit numeric ID where each digit corresponds to the numeric value (1 to 8) assigned to the adverb of time characterizing the occurrences of the"Strong Green Vegetation", the"Weak Green Vegetation" and the"Brown Mineral" classes of *Colour-Material*, respectively. Consequently, the numeric IDs range from 111 for pixels never classified in any of these three classes of *colour-Material* to 888 for pixels always classified in each of these three classes of *colour-Materials* (which is actually an impossible case).

Finally, since the number of modular classes is potentially very high, we assigned colours to every class automatically in order to ease the map visualization. For this purpose, we defined one reference colour, i.e."darkgreen","yellow3" and"tan4" as defined in the R environment, for each of the three classes of *colour-material* used at the modular stage, i.e."Strong Green Vegetation","Weak Green Vegetation" and"Brown Mineral" respectively. These reference colours were then converted to RGB colour space and mixed proportionally to the occurrences of their corresponding classes in order to compute a new colour for each modular class. For example, the modular class"345 - SOM-SGV / REG-WGV / PRED-BM" (i.e. sometimes (10–25%) Strong Green Vegetation, regularly (25–50%) Weak Green Vegetation and predominantly (50–75%) Brown Mineral) will be assigned a RGB colour that mixes: 1) 17.5% (midpoint between 10 and 25%) of"darkgreen" ($r = 0$, g = 100, b = 0) with 2) 37.5% (midpoint between 25 and 50%) of"yellow3" (r = 205, g = 205, b = 0) and 3) 62.5% (midpoint between 50 and 75%) of"tan4" (r = 139, g = 90, b = 43). The RGB values of the resulting colour are then (see Eq. (8) and corresponding colour in fourth line of Table 6):

$$\begin{cases} r = (0.175*0 + 0.375*205 + 0.625*139)/(0.175 + 0.375 + 0.625) = 139 \\ g = (0.175*100 + 0.375*205 + 0.625*90)/(0.175 + 0.375 + 0.625) = 128 \\ b = (0.175*0 + 0.375*0 + 0.625*43)/(0.175 + 0.375 + 0.625) = 23 \end{cases} \quad (8)$$

Examples of modular classes and their associated colours are shown in Table 6. We also introduce potential land cover classes associated with the vegetation gradient. Browner colours refer to high occurrences of Brown Mineral classes of *colour-material* and are thus expected to correspond to permanent bare soils or urban areas (see also Supplementary Material 5). Crops are expected to be associated to mixed occurrences of Strong Green Vegetation and Brown Mineral classes. Herbaceous vegetation (pasture and open cerrado) with a longer vegetative cycle than crops and low biomass should be represented by yellow-green colours corresponding to high occurrences of Weak Green Vegetation. Woody vegetation is represented by greener colours due to higher occurrences of Strong Green Vegetation. Finally, evergreen forests should correspond to dark green colours corresponding to always Strong Green Vegetation.

3.4. From image classification to thematic application

The final classifications were analysed to assess how they could benefit the end-users with regards to their specific applications. In the present case, the situation is straightforward since the end-user's requirement consists in mapping land cover classes (natural vegetation, with focus on riparian forests, and water bodies), whose accuracy can then be assessed by comparing the classifications with reference land cover maps. In this regard, we used different reference data sets provided by the end-users and thus containing the main classes of interest according to their requirements.

3.4.1. Natural vegetation

At first, we aimed to assess how efficient the automatic approach was to map areas of natural vegetation. To do so, we relied on the 2008 map of consolidated rural areas (CRA) produced by ICV based on photo-interpretation of high resolution images (SPOT 5 images at 2.5 m spatial resolution) for the entire state of Mato Grosso. We then crossed that map with additional information in order to map remnants of natural vegetation in 2017 (hereafter named NatVeg2017), i.e. at the date of acquisition of the Sentinel-2 images. For this purpose, we used 1) the annual official deforestation maps provided by INPE (Brazilian National Institute for Space Research) through the PRODES program (the Brazilian Deforestation Monitoring Program) and 2) the 2017 MapBiomas land cover map (Collection 5) produced by a multidisciplinary team based on supervised classification of Landsat time series on Google Earth Engine. Areas of natural vegetation in 2017 were then defined as areas that were 1) neither considered as consolidated in 2008, 2) nor deforested between 2008 and 2017 according to PRODES maps, 3) nor classified as water or urban in MapBiomas 2017. We then randomly selected 500 validation point samples in each Sentinel-2 tile and retrieved their reference labels in the NatVeg2017 map and in the corresponding modular classifications in order to compute traditional validation statistical indices such as the F-score. By doing so, we intended to analyze the spatial heterogeneity of the classification accuracy across the study area.

Yet, beyond the statistical validation, we also wished to underline to the end-user that, although the reference map (NatVeg2017 map) is unique, various potentially accurate land cover classifications can be produced. In other words, various correct interpretations of a unique dataset of satellite images can coexist, thus illustrating the vagueness issue of geographic terms as mentioned in Section 1.1. For example, the validation of the natural vegetation land cover class was challenging since our approach did not produce an explicitly defined class of"Natural Vegetation" at the modular stage. Indeed, we rather mapped a gradient of terrestrial vegetation classes. Considering that most tropical native vegetation in the study is evergreen, we focused on the modular classes that were"never" or"rarely" observed as"Brown Mineral" *Colour-Material*. We ordered them in a gradient ranging from classes corresponding to pixels only classified in"Strong Green Vegetation" (i.e. IDs 811, 711, 611, 511, 411, 311, 211) on the one side, to classes referring to pixels only classified in"Weak Green Vegetation" (i.e. IDS 181,171,161,151,141,131,121), on the other side. It is worth noting that classes with little total occurrences in all classes of *colour-material* taken into account at the modular stage (e.g. $ID = 211$ or $ID = 121$) had more observations in the"Blue Water" *colour-material* but not enough to be classified as"Aquatic". Between these two extremes, the modular classes were ordered according to their decreasing occurrences of"Strong Green Vegetation" and increasing occurrences of"Weak Green Vegetation". Based on this gradient, we then iteratively computed the F-score comparing the reference labels (retrieved from the NatVeg2017 map) of the 500 randomly selected points in each Sentinel-2 tile with the various

potential masks of natural vegetation computed by integrating a new class of the gradient at each new iteration until all classes of the gradient were considered. By doing so, we intended to set the optimal combination of modular classes that would best discriminate areas of natural vegetation according to the end-user's definition.

In order to take the analysis of natural vegetation maps one step further, we then focused on the potential of our approach to estimate the level of degradation of riparian forests in Permament Protected Areas (PPA). For this specific task, we used four different reference land cover maps from 2016 (hereafter named LC2016_4) provided by the ICV NGO for four municipalities (Alta Floresta, Carlinda, CotriguaÃ§u and Paranaita) and with detailed information about native vegetation, PPA and associated water bodies. These maps were also produced by visual interpretation of very high resolution data (SPOT 5 images at 2.5 m spatial resolution). Finally, we assessed the effectiveness of the approach to assist the end-users in monitoring vegetation degradation in riparian protected areas by comparing the proportion of degraded riparian forests as measured by the end-user and as estimated by the system, using different thresholds in the vegetation gradient, for $N = 1{,}239$ watersheds delineated by the Brazilian National Water Agency (ANA).

3.4.2. Water bodies

With regard to the mapping of water bodies, we used recent (2016) reference land cover maps provided by the end-user for 18 municipalities in northern Mato Grosso (hereafter named LC2016_18). These maps are similar to LC2016_4 except they do not contain information on the delineation of PPA and thus cannot be used to validate riparian forests. But, LC2016_18 maps contain many information on the location of natural and artificial water bodies and can thus be used to assess the potential of the approach to map this class. For this reason, we compared the"Water" samples from the reference data with their corresponding pixel values produced at the dichotomous stage, either considering only the"Water" class or both classes of"Water" and"Aquatic Vegetation". In addition, since the width of water courses was informed by the end-users in the database,

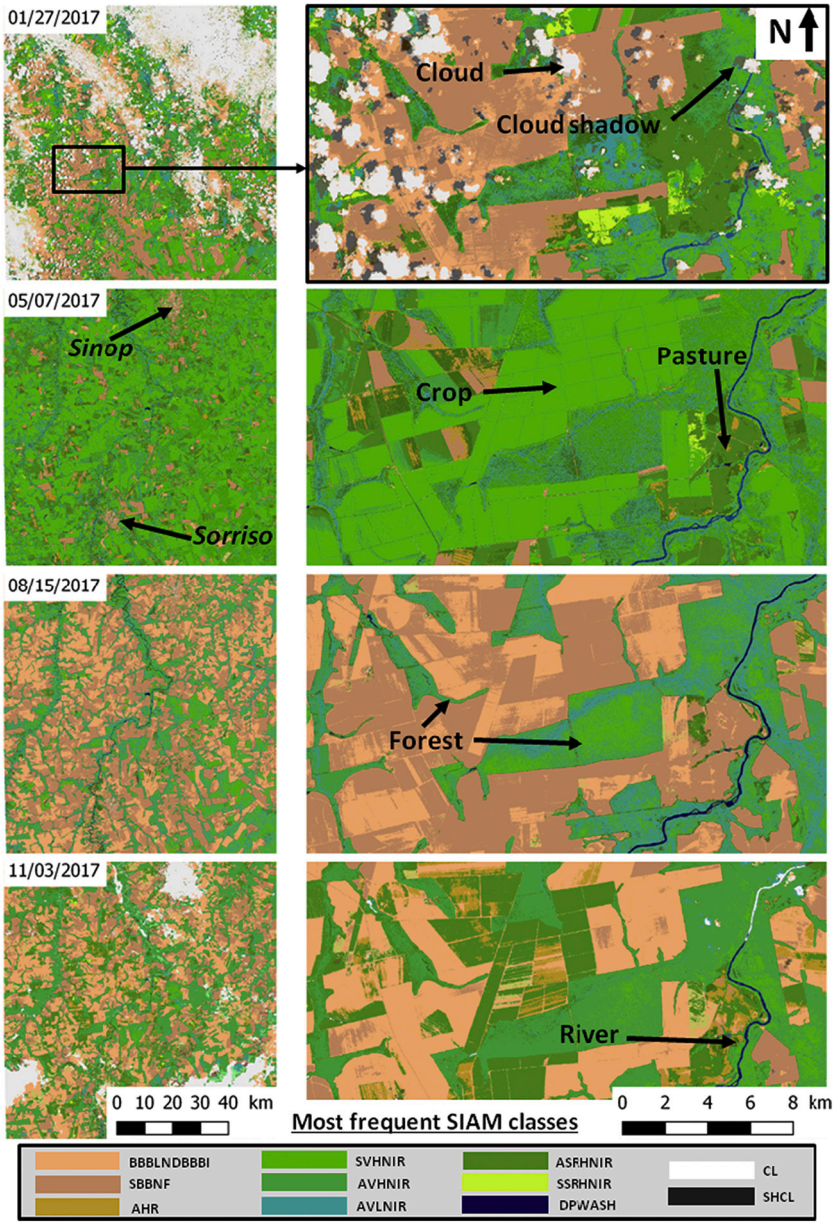

Fig. 6. Examples of SIAM classifications (Tile 21LXG) at four different dates. The complete legend is in Table 3.

it was possible to assess the effectiveness of the system to map different sizes of water bodies. In this regard, we applied iterative internal buffers (of 10 m to 100 m by 10 m step) to collect new water samples and thus plot the evolution of validation statistics in function of the size of water bodies.

4. Results

4.1. Observables

The SIAM classifier was applied on the 2069 Sentinel-2 images in order to map spectral categories and their associated classes of *Colour-Material* (Table 3). Some resulting examples are shown in Fig. 6 for one tile (21LXG) located in central Mato Grosso between the cities of Sorriso and Sinop. For this specific tile, 20 images were acquired but only four SIAM maps corresponding to different months (January, May, August and November) are shown here. They illustrate the ability of the approach to detect clouds and cloud-shadows and to monitor the seasonal evolution of vegetation phenology (which follows the rainy season from September to May). Indeed, forests remain green throughout the year whereas other vegetation covers (i.e. mainly crops and pastures) are represented with changing colours (from brown to green). In the present case covering a large farm specialized in both cattle ranching and crop cultivation (soybean, maize and cotton), 1) the January image corresponds to the soybean harvest followed by the planting of cotton and maize thus explaining the large presence of bare soils in crop fields whereas pastures and forests are green, 2) the May image corresponds to

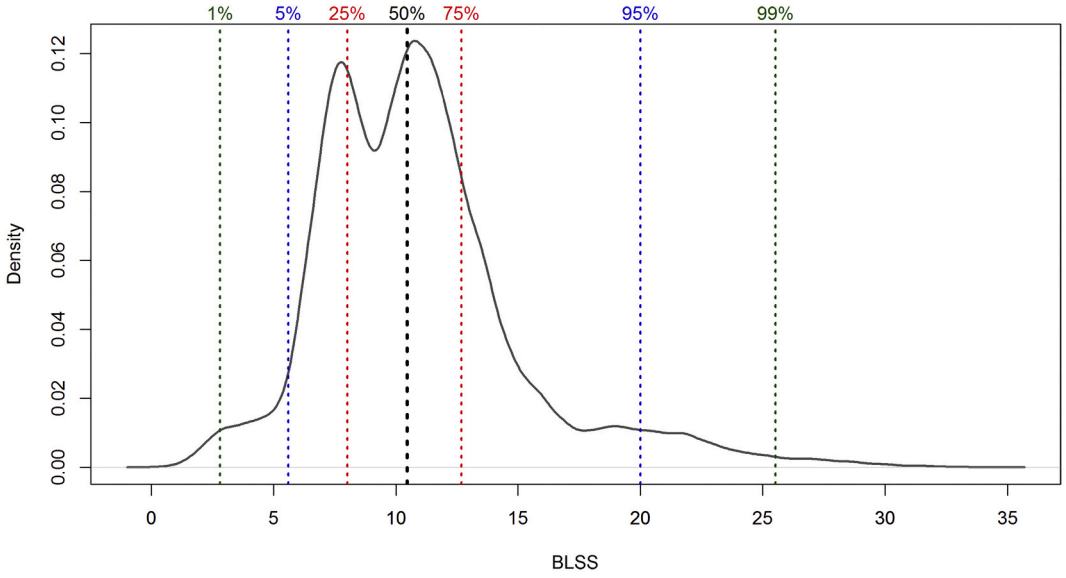

Fig. 7. Density function of BLSS values.

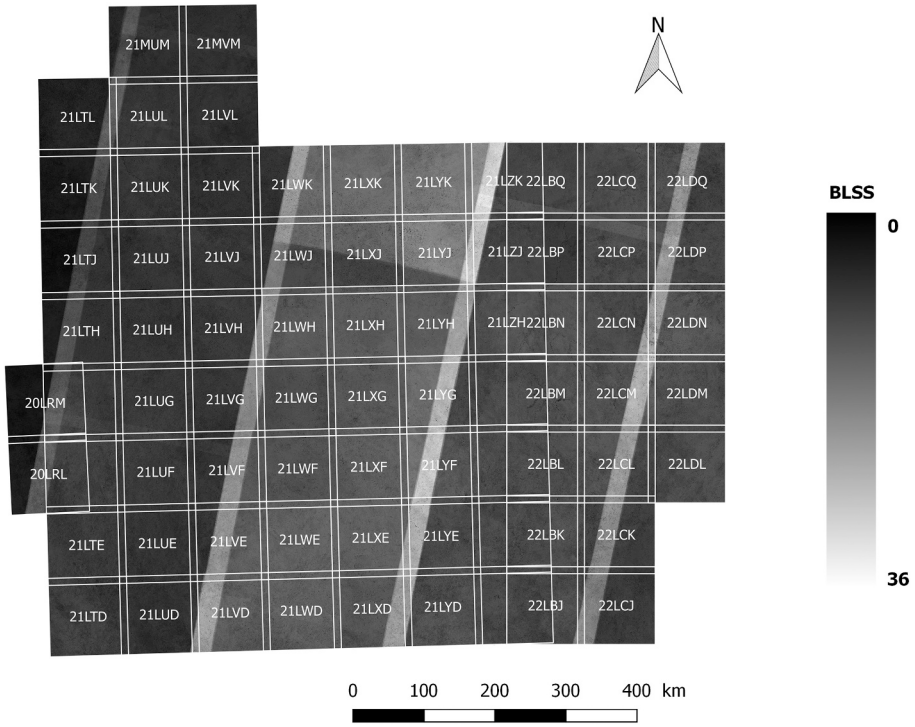

Fig. 8. Map of best land surface scores (BLSS).

a period of high photosynthetic activity in cotton and maize fields so that crop fields are as green as forested areas whereas pastures are in weak green, 3) the August image corresponds to the end of the dry season when no crop is photosynthetically active while forests (including riparian forests) remain green and 4) the November image corresponds to the beginning of the soybean vegetation cycle with crops appearing as weak green or even bare soil depending on the planting date. To summarize, forests remain green throughout the year whereas other vegetation covers (i.e. crops and pastures mainly) characterized by a strong phenological cycle are represented with changing colours (from brown to green). Finally, the water bodies such as the Teles Pires river, are mapped in blue in all images.

4.2. Similarities

We computed the scores for all classes of *colour-material* and then derived the Best Possible Score (BPS), Best Land Surface Score (BLSS) and the Scores of *Colour-Material* classes for all pixels of the study area.

The Best Possible Score (BPS) refers to the best score that could be assigned to a pixel being always classified in the same class of *Colour-Material*. The Best Land Surface Score (BLSS) approximates to BPS except it only considers classes of *Colour-Material* related to land surfaces, i.e. disregarding"Black Shadow" and"White Cloud". Thus, BPS is higher or equal to BLSS and the higher is the difference between BPS and BLSS, the higher is the presence of clouds and/or shadows in the time series. Values range from 3.76 (at tile 21LTJ) to 36.95 (at tile LZK) for BPS and from 0 to 35.87 for BLSS. With respect to the latter, the density function (Fig. 7) indicates that 50% of pixels have a BLSS value between 8 and 12.7, thus benefiting from a significant number of observation. In addition, 1% of pixels have a value below 2.8 (i.e. being rarely observed) and 5% present a value greater than 20 (i.e. being often observed). Moreover, both BPS (not shown) and BLSS (Fig. 8) show similar spatial patterns. At a regional scale, a east-west gradient can be noticed with lower values in western areas (Tiles 21LTL, 21LTK) corresponding to areas with very high cloud cover rates and/or missing data affecting the quality of image time series. At local scale, highest values correspond to overlapping areas at the border between two satellite swaths so that discrepancies inside Sentinel-2 tiles also appear. For example, tiles

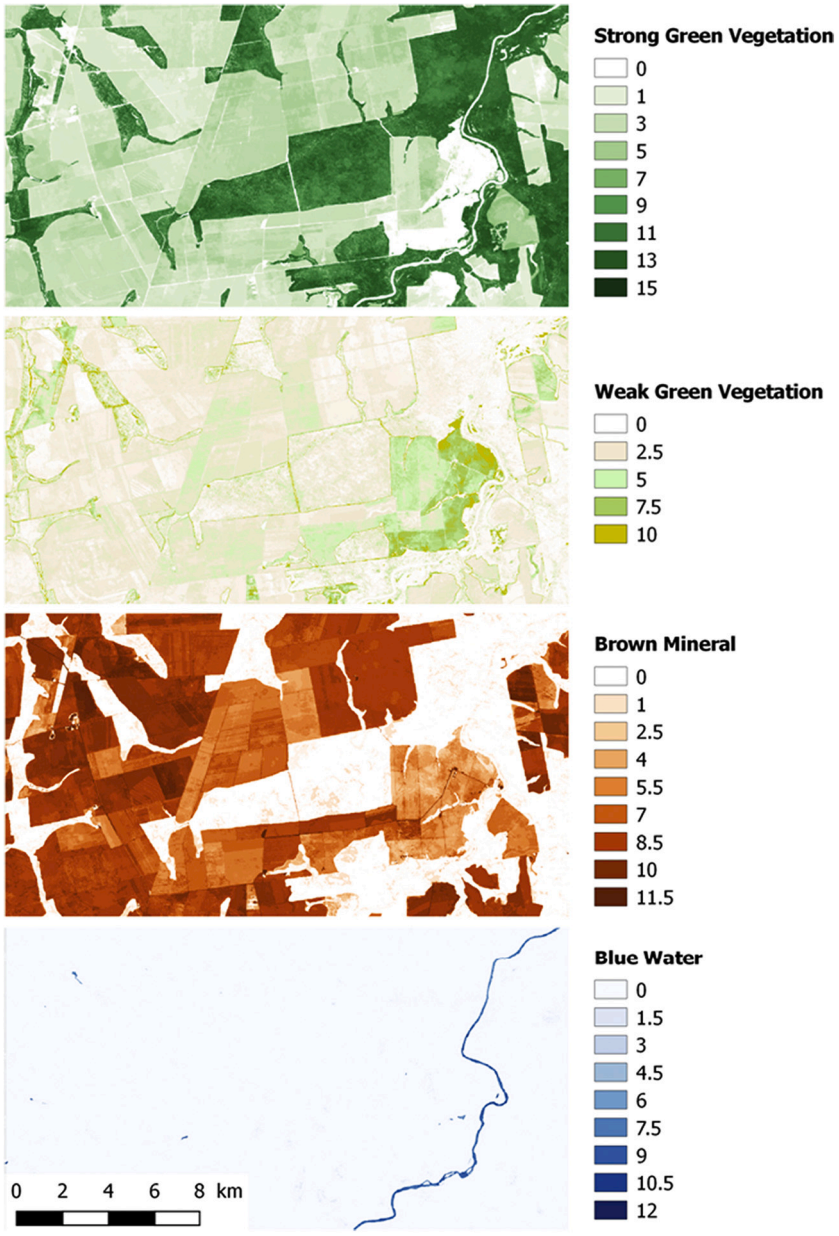

Fig. 9. Examples of scores measured for the main classes of *Colour-Material* (Tile 21LXG).

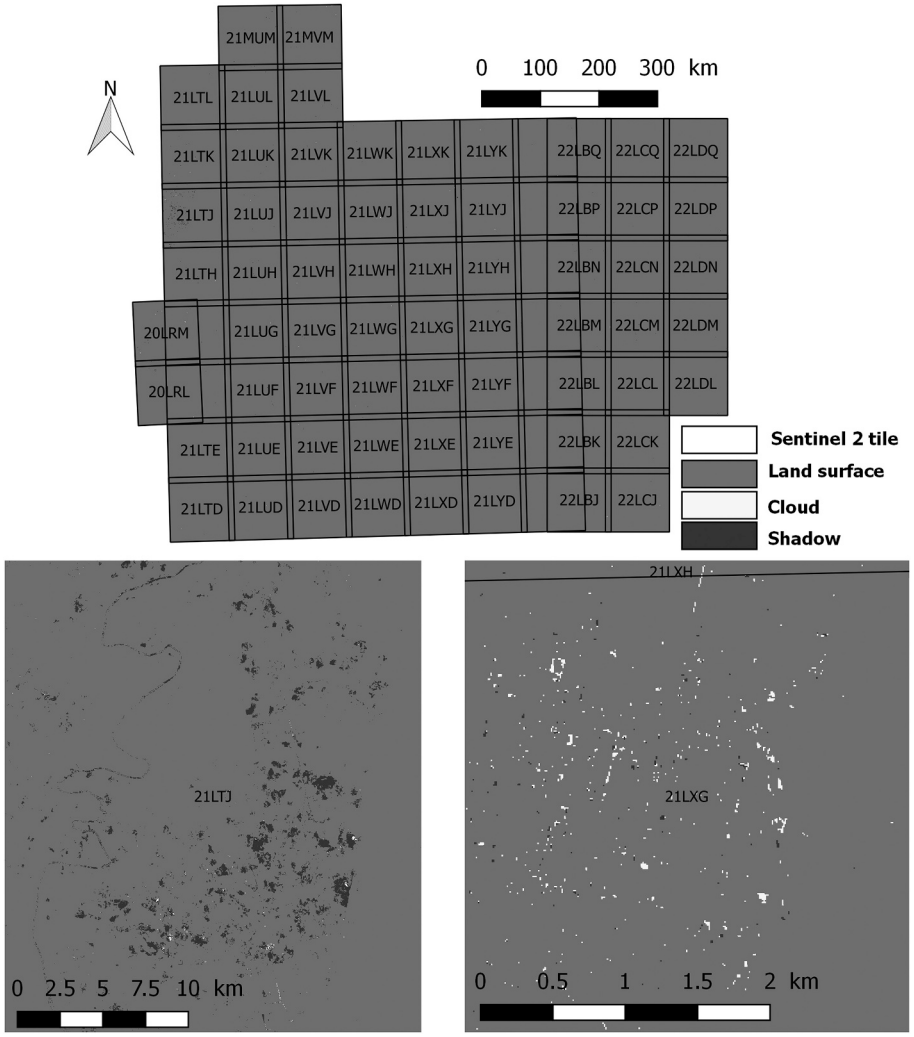

Fig. 10. Map produced at the initial stage with minor entities, i.e. land surfaces, clouds and shadows.

21LWL or 21LWK show much lower values in western areas than in eastern areas.

Finally, the Fig. 9 shows the scores for the main classes of *Colour-Material* related to land surfaces at a same location in central Mato Grosso. High scores of"Strong Green Vegetation" correspond to evergreen forests with high vegetative activity throughout the year whereas high scores of"Weak Strong Vegetation" refer to pastures or sparse natural vegetation (i.e. Cerrado). Crop fields are represented with moderate to high scores of"Brown Mineral" due to the over representation of dry season images in the time series. High scores in"Blue Water" emphasize the presence of natural or artificial water bodies. Also, it is worth mentioning that, as observed in Fig. 8, the overlapping areas have higher values in every score images (although not shown in Fig. 9) since scores are absolute values whose computation depends on the length and quality of the image time series. Yet, these areas are not processed differently in the next steps of the system since the classification rules are based on normalized occurrences (in percent) as expressed in Eq. (4) and Table 4.

4.3. Classifications

We here introduce the classifications obtained at the initial, dichotomous and modular stages. The statistical analysis for validation is then introduced in Section 4.4.

4.3.1. Initial stage

The Fig. 10 introduces the map produced at the initial stage of the approach to discriminate minor entities, i.e. land surfaces, clouds and shadows. A large majority (99.96%) of pixels were classified as"Land Surface" confirming the possibility to produce a final (nearly) cloud-free map. Clouds (0.0055%) and shadows (0.03%) represented very little portions of the entire study area. Most shadows were encountered in a few tiles with low quality image time series (e.g. 21LTJ) or in urban areas where high buildings can be associated to projected shadows. Similarly, most cloud pixels were found in urban areas, where buildings' roofs made of very reflective material (e.g. storage sheds) were confused with clouds.

4.3.2. Dichotomous stage

At the dichotomous stage, land surfaces were discriminated in four major land surface material types, i.e. Terrestrial Vegetation, Mineral, Aquatic Vegetation and Water (Fig. 11). The results show the predominance of terrestrial vegetation (98.66% of pixels classified as land surfaces at the initial stage), which includes both natural (i.e. forest and cerrado) and managed (crops and pastures) vegetation. Mineral areas covered 0.92% of the study area, mainly corresponding to urban areas (such as Sinop in tile 21LXG and Campo Novo do Parecis in tile 21LUF) or bare soils (as in tile 21LVE). Bare soils may correspond to fallow fields or cultivated fields that, for some reason (e.g. very high cloud cover rates during the rainy season), were only observed during the dry season

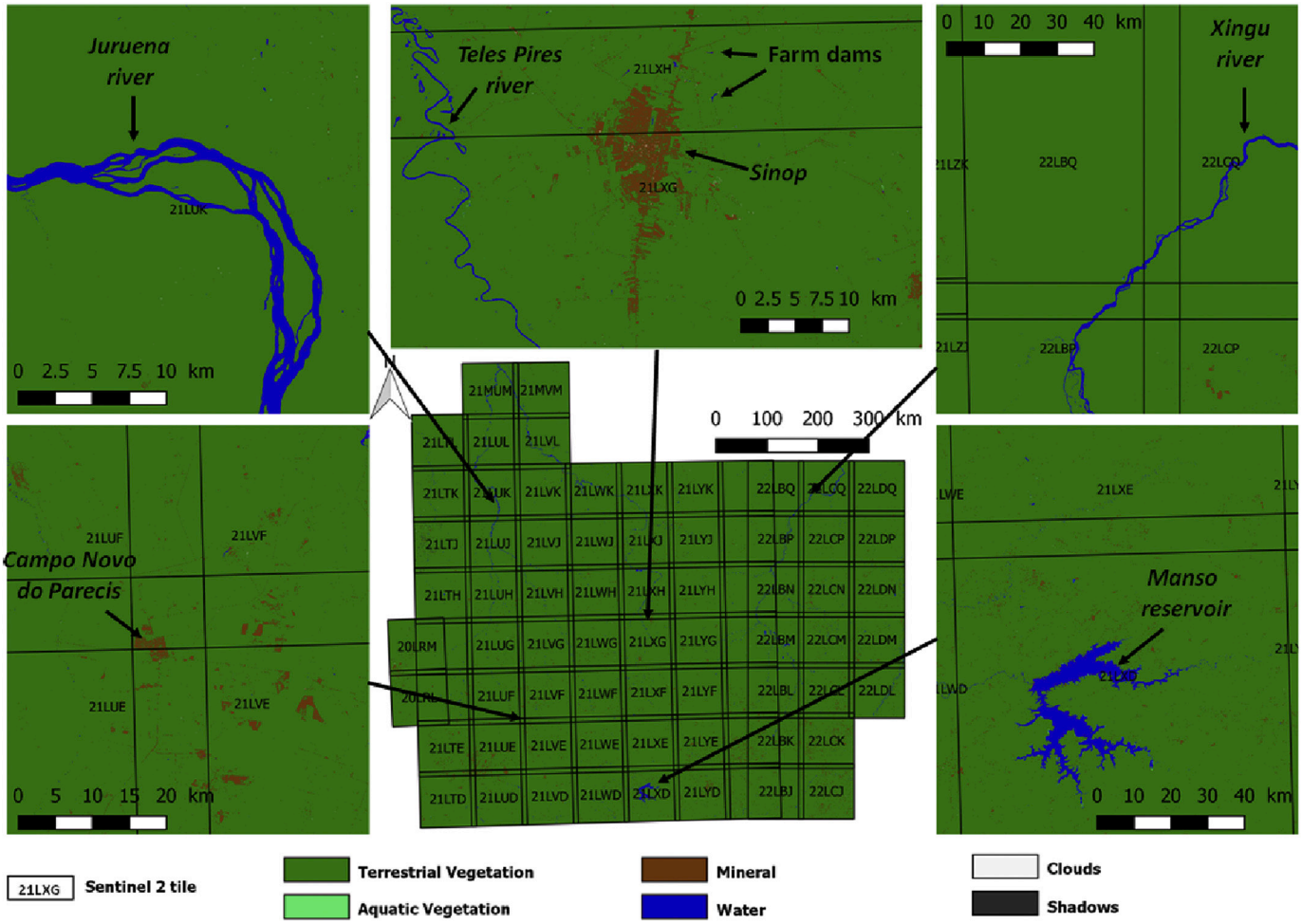

Fig. 11. Map produced at the dichotomous stage with Land Surface Material Types.

when there was no standing crop. Water bodies represented 0.4% of the land surfaces, including rivers (as in tiles 21LUK, 21LXG and 22LBQ representing the main rivers in the study area) and small (tile 21LXG) or large artificial dams (as the Manso hydropower reservoir in tile 21LXD). Finally, only 0.011% of land surfaces were classified as"Aquatic Vegetation" corresponding to pixels in wetlands or at the banks of water bodies.

4.3.3. Modular stage

At the modular stage, pixels classified as"Terrestrial Vegetation" were further described with additional characteristics regarding the occurrences of"Strong Green Vegetation","Weak Green Vegetation" and"Brown Mineral" classes of *Colour-Material*. At the end, 142 modular classes were encountered thus representing a large diversity of combinations. Nonetheless, the 20 most represented classes covered 87.8% of the total of"Terrestrial Vegetation" pixels (each of these 20 classes accounted for more than 1% of the total number of pixels). The distributions of these 20 classes, their label descriptions and their associated colours are shown in Fig. 12 and evidence the importance of 4 classes (811, 711, 154 and 145) which accounted for 53.1% of all"Terrestrial Vegetation" pixels. The Fig. 12 serves as a legend to understand the map produced at the modular stage (Fig. 13). At regional scale, the SE-NW vegetation gradient from Cerrado to rain forests appeared clearly. Pasture areas (tiles 21LUK, 21LXG and 22LCP) were classified with similar colour shades than cerrado areas (tiles 21LXD and 21LUE). This is because they actually both correspond to herbaceous land cover with sparse shrubs or trees. Crops were assigned to brown-green colour shades (e.g. as classes 335 or 415 in Fig. 12) corresponding to a mix of all classes of *Colour-Material* throughout the year. Finally, forests appeared in dark green. It is also worth noting that other classes discriminated at the dichotomous stage ("Water","Mineral" and"Aquatic Vegetation") were preserved at the modular stage.

4.4. From image classification to thematic application

4.4.1. Water bodies

The Fig. 14 shows subsets of classifications obtained at the modular stage and focused on water bodies. Main river courses such as Juruena (Fig. 14A) and Xingu rivers (Fig. 14D) were mapped, evidencing cases of anastomosis (Fig. 14A) or the presence of temporary river banks emerging during the dry season (mapped as Mineral in Fig. 14D). Similarly, large reservoirs were correctly delineated, as it was the case for the Teles Pires hydropower reservoir (Fig. 14B). Overall, small natural and artificial water bodies were captured, as it was the case for excavated tanks for fish farming (Fig. 14C), small farm dams (Fig. 14E) or natural lakes in Cerrado areas (Fig. 14F).

After visual assessment, the accuracy of the approach to map water bodies was also validated using the F-score statistical index (Table 7). Reference samples were extracted from land use maps produced by the end users (LC2016_18) and compared with the dichotomous classification. More specifically, two definitions of"Water" were considered, i.e. a restrictive definition considering only the"Water" class and a broad definition considering both classes of"Water" and"Aquatic Vegetation". F-scores were always better when considering both classes of"Water" and"Aquatic Vegetation" as water bodies. As expected, the lowest F-scores ($F = 0.802$) were obtained when using all reference samples, i.e.

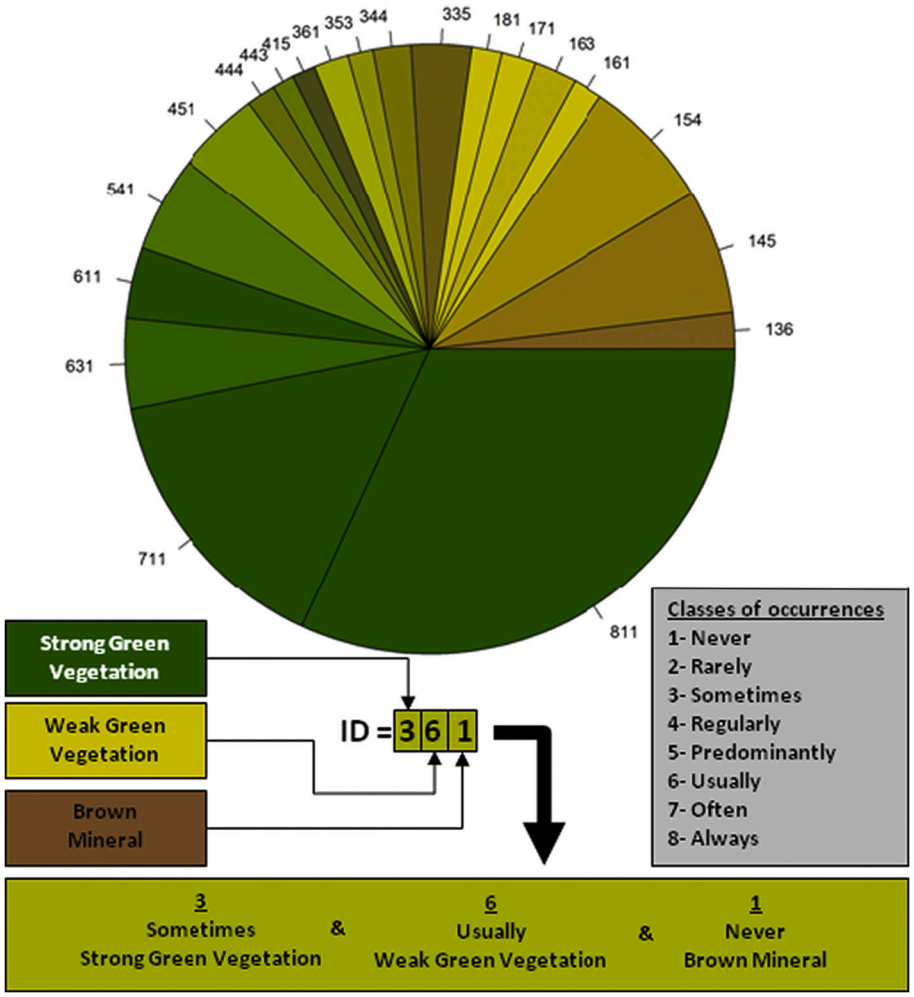

Fig. 12. Distribution of the 20 most represented modular classes with their label descriptions and associated colours.

including very small water bodies (< 10 m width) or hidden by the canopy. Then, the results improved significantly when focusing on water bodies larger than 10 m (F = 0.874), 20 m (F = 0.927) or even 100 m (F = 0.961), i.e. when considering that only water bodies larger than the image spatial resolution (10 m) can"exist" in Sentinel-2 images (see Section 2.2.1 about the existence stage of the semantic contraction proposed by Couclelis (Couclelis, 2010)).

4.4.2. Natural vegetation

The validation of the"Natural Vegetation" class was performed by comparing the modular classes retrieved at 500 random samples per tile (N = 37,500 samples for the entire study area) with the corresponding values in the reference NatVeg2017 map. The validation also intended to define the best combination of modular classes approximating the reference map. Considering that most natural vegetation in the study area is made of evergreen vegetation, we focused on the modular classes that were"never" or"rarely" observed as"Brown Mineral" *Colour-Material*, i.e. 41 classes out of a total of 142. These classes were then sorted according to a vegetation gradient ranging from"Always Strong Green Vegetation" (ID = 811) to"Always Weak Green Vegetation" (ID = 181), i.e. from the greenest to the yellowest classes. Combinations of modular classes were then tested iteratively including a new class at each iteration. Fig. 15 shows the evolution of the F-score for each combination of modular classes. The high F-score values (>0.8) achieved with all combinations indicated it did not exist a unique combination of classes to represent the areas of natural vegetation as originally delineated by the end-users. Interestingly, the F-score achieves its maximum value (F = 0.875) when considering all modular classes, i.e. pixels that are only classified as"Green Vegetation", either"Strong" or"Weak". This means that including modular classes with occurrences of "Brown Mineral" may potentially improve the mapping of natural vegetation. This is confirmed when analyzing the spatial variability of accuracy metrics across the study area (Fig. 16) evidencing lower F-score values (e.g. F = 0.68 in Tile 21LCJ) in southern areas dominated by open savannas which can be confused with bare soil during the dry season. On the contrary, dense rainforests in northern areas are better classified (F > 0.9) and considering less combinations of modular classes such as in tiles 21LWK and 21LYG (Figs. 15 and 16). Yet, it is worth mentioning that few areas achieved very high F-score values (F = 1) when considering all combinations of modular classes. These areas actually correspond to protected areas (e.g. conservation units or indigenous lands) where small non forested areas (i.e. yellowest classes in the colour gradient) may still correspond to natural vegetation.

In order to illustrate the implications of changing the combination of modular classes in the mapping of natural vegetation, we set five thresholds (NV1 to NV5) in the colour gradient of modular classes (Fig. 15) corresponding to five different definitions, ranging from a restrictive definition of natural vegetation corresponding to pixels always classified as "Strong Green Vegetation" to an open definition of natural vegetation considering all pixels always classified as"Green Vegetation", either"Strong" or"Weak". The natural language definitions corresponding to these five combinations are expressed in Table 8. We then identified four examples illustrating the importance to consider vegetation gradients when monitoring fine changes in vegetation cover.

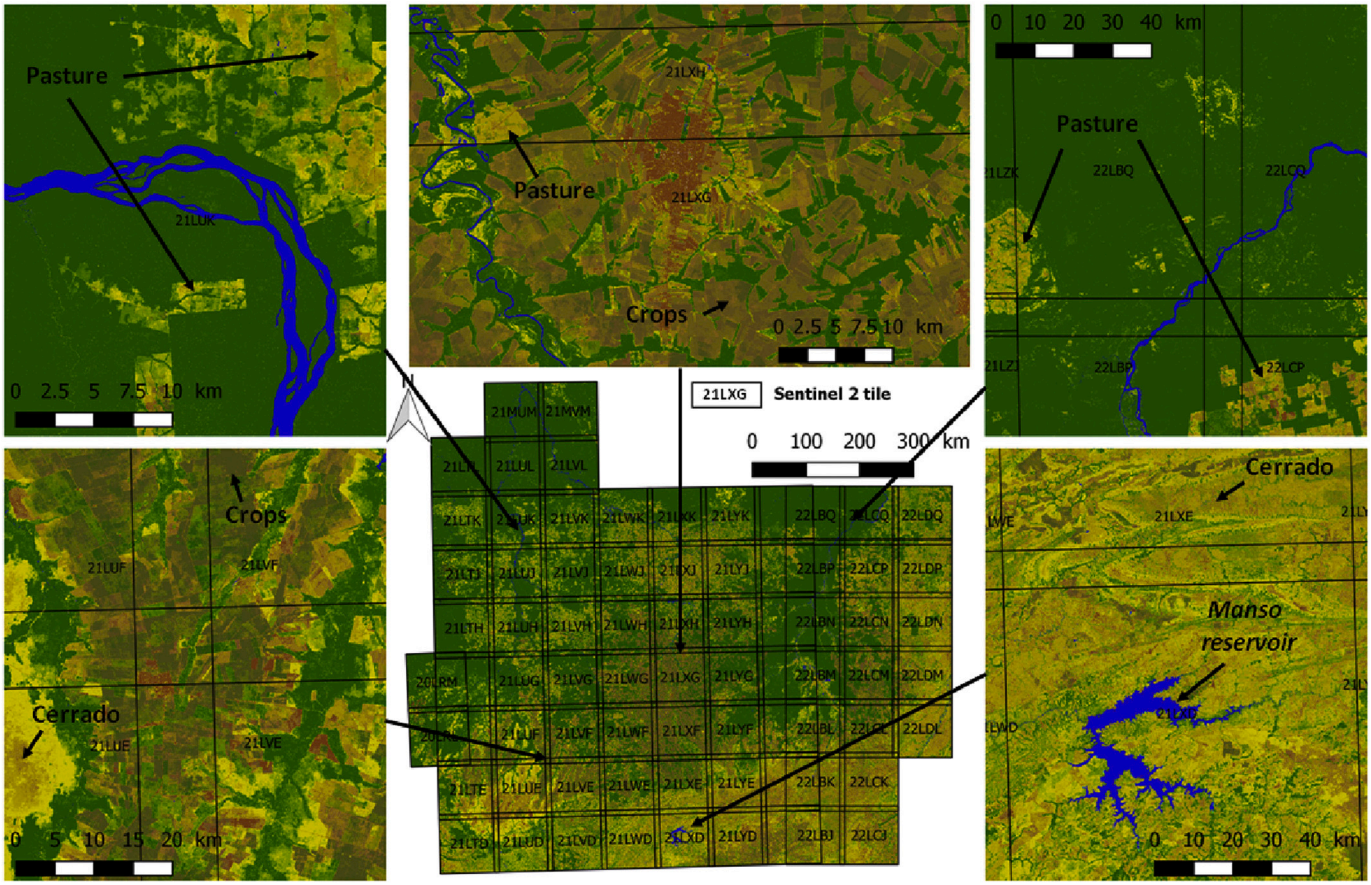

Fig. 13. Map produced at the modular stage.

The first example (Fig. 17A) is centered around an area of degraded forest and shows the difficulty to accurately delineate forest patches. At NV1 (restrictive definition), degraded areas are discarded and forest patches are discontinuous whereas, at NV5 (Open definition), degraded areas are classified as forests and connectivity is preserved. Similar conclusions can be drawn from Fig. 17B centered on a logged forest. At NV1, forests appear as highly fragmented and degraded. At NV2 (Closed), NV3 (Intermediate) and NV4 (Broad), only the human infrastructures (logging roads and log landings) are discriminated. At NV5, the entire area is considered as forest. In Fig. 17C, humid riparian forests are surrounded by dry forests and Cerrado areas on neighboring plateaus. Here again, the maps differ dramatically from NV1 to NV5 with Cerrado areas being totally included in the mask of natural vegetation at NV5. Finally, Fig. 17D shows how the extension of an indigenous village (*Camaiura*, inside the Xingu indigenous land) with traditional slash-and-burn agriculture varies depending on the chosen definition of natural vegetation.

In addition, it is necessary to better assess the quality of the maps of natural vegetation for local scale applications, especially regarding the end-users interest in mapping degraded riparian forests in Permanently Protected Areas (PPA) according to the Brazilian Forest Code. For this purpose, we compared the proportion of degraded areas measured by the end-users through visual interpretation for $N = 1{,}239$ watersheds in Northern Mato Grosso with the corresponding estimates produced at modular stage (Fig. 18). As expected, the restrictive maps of natural vegetation (NV1) tended to overestimate degradation whereas the open forest maps (NV5) underestimated degradation. The highest correlation ($R^2 = 0.841$) was achieved with the closed map (NV2), which means that this definition could be used on a regular basis to produce rapid updates on vegetation degradation in riparian Permanent Protected Areas.

5. Discussion

The knowledge-driven method proposed in this paper relies on two main pillars: 1) a robust conceptual framework to guide the system's architecture and 2) the implementation of the system per se with regard to a specific application. Here we first discuss the limitations of the current implementation of the system in order to set out future prospects for improvement of the conceptual framework. Finally, we discuss how the approach could contribute to reducing the gap between remote sensing and end-user expert knowledge.

5.1. The system's implementation

As for today, the system highly depends on the SIAM algorithm (Baraldi et al., 2006) to efficiently discriminate *Observable* characteristics, i.e. to classify main classes of *Colour-Material*. SIAM works with top-of-atmosphere (TOARF) or surface reflectance values (SURF), the latter being an ideal case of the former (Baraldi et al., 2010). In this study, we used TOARF data but we intend to consider how SURF data would improve the final classifications. Second, SIAM actually differentiates much more spectral categories (Table 3) that shall be further analysed in order to identify additional classes of *Colour-Material* and consequently other land surface material types. For example, the"Brown Mineral" *Colour-Material* could be split in various sub-classes as done for the"-Green Vegetation" classes. Conversely, other potentially interesting classes of *Colour-Material* were not discriminated by SIAM. For example, green cotton fields display higher NIR values than forested areas but both are classified as"Strong Green Vegetation" *Colour-Material*. This latter class is actually over represented in tropical forested areas since it can be assigned to many different vegetation types (i.e. forests, crops, pastures) depending on the date of the year. To address this issue, we

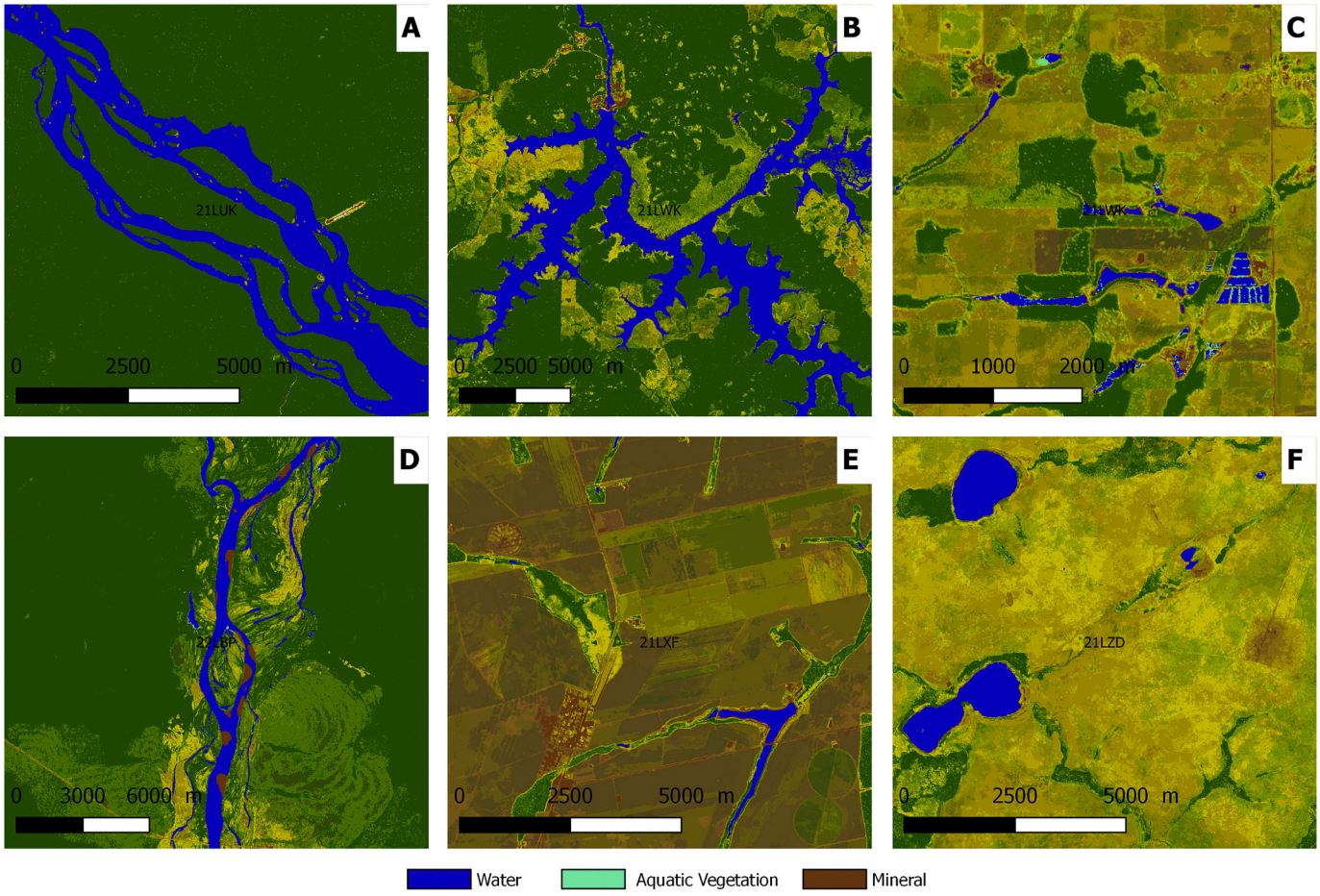

Fig. 14. Examples of detection of water bodies.

Table 7
F-score validation statistics for water bodies.

	Minimum width of water bodies										
	All	10 m	20 m	30 m	40 m	50 m	60 m	70 m	80 m	90 m	100 m
Water	0.802	0.867	0.918	0.934	0.938	0.920	0.944	0.947	0.960	0.961	0.960
Water + Aqu. Veg.	0.808	0.874	0.927	0.938	0.942	0.926	0.946	0.951	0.965	0.962	0.961
N	1000	1000	1000	1000	1000	1000	1000	1000	820	626	495

consider that the potential of the red-edge bands of Sentinel-2 images should be further explored to better discriminate vegetation classes (Lin et al., 2019). Finally, texture is another *Sense Qualia* observable characteristic whose effectiveness to improve land cover classification has long been studied, especially in tropical forests (Lu, 2005). But integrating texture in the approach would first require categorizing it in a robust manner. In this regard, the FOTO approach (Couteron et al., 2005) can serve as an inspiration although it does not yet assign semantic labels to the texture classes. Texture could also be derived from other data such as Sentinel 1 since sensibility of SAR images to land surface roughness has long been studied (Lee and Pottier, 2009). In addition, using SAR images would also be useful to complete the time series, especially during the rainy season since the scoring approach resulted in giving more importance to dry season optical images (from May to September). However, in order to ensure the overall consistency of the approach, it would be necessary to rely on a similar approach than SIAM but adapted to SAR data, which does not exist to date.

With regard to *Similarities*, we only focused on one measurable information referring to the occurrences of *Colour-Material* classes as this information was considered sufficient to map the classes of interest (i.e. forests and water bodies). Yet, in the current version of the system, the counting of occurrences is weighted by the quality of the images that compose the time series considering their cloud cover percentage measured at tile-level. By doing so, the spatial distribution of pixel's quality in an image is not taken into account since a unique weight is assigned to all pixels. In order to overcome that issue, we wish to test the feasibility to assign pixel-based weights based on the distance to clouds and shadows. But overall, other similarities related to temporal patterns may be computed to derive additional modular classes representing land cover trajectories as expressed by Câmara (Câmara, 2020). For example, it may consist in computing other knowledge-based temporal features to map annual croplands (e.g. maximum value in the red band, maximum NDVI, minimum NDVI, maximum positive NDVI slope and maximum negative NDVI slope as in (Waldner et al., 2015; Arvor et al., 2011)) or including endmembers fraction resulting from linear unmixing models regularly used to map forest degradation or stages of forest regeneration in the Amazon (Bullock et al., 2020; Asner, 2009; Lu, 2003).But, the accuracy of such temporal features also depends on the completeness of

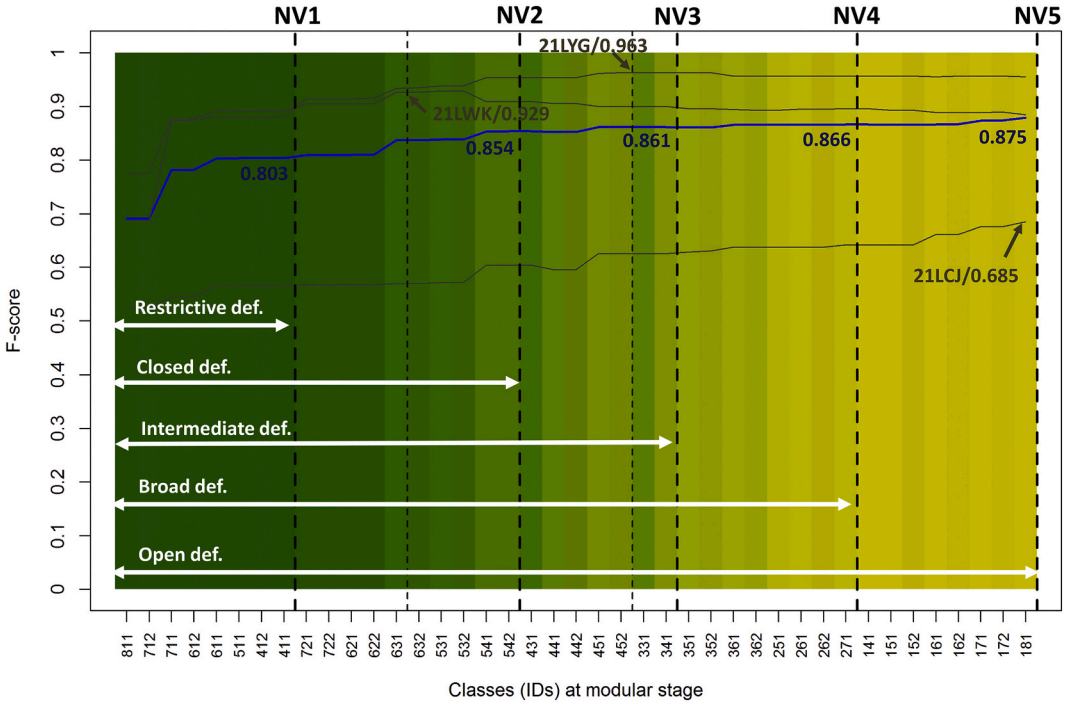

Fig. 15. Validation of the natural vegetation land cover class with F-score statistics computed for various combinations of modular classes.

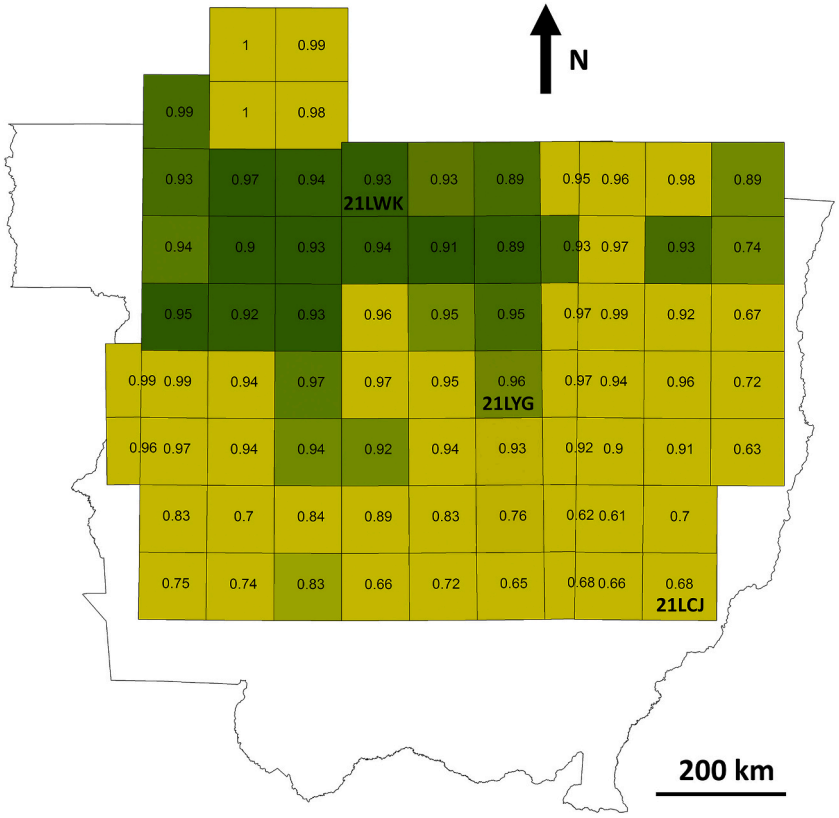

Fig. 16. Validation of the natural vegetation land cover class with F-score statistics for each Sentinel-2 tile. The colour corresponds to the threshold in the colour gradient (see Fig. 15) at which the best F-score value was achieved.

Table 8
Natural language definitions of the five potential classes of natural vegetation identified in Fig. 15.

Label	Natural language definition
	A pixel represents a Natural Vegetation if that pixel is…
NV1- Restrictive	…Always Strong Green Vegetation
NV2- Closed	…(At least) Predominantly Strong Green Vegetation and Never or Rarely Brown Mineral
NV3- Intermediate	…(At most) Regularly Strong Green Vegetation and (at most) Regularly Weak Green Vegetation and Never or Rarely Brown Mineral
NV4- Broad	…(At least) Rarely Strong Green Vegetation and Never or Rarely Brown Mineral
NV5- Open	…Always Strong or Weak Green Vegetation

the input time series, which usually suffer from spatial inhomogeneity (Sudmanns et al., 2019). In addition, spatial similarities (e.g. patch geometry) and spatial or temporal relations between geographic objects may allow identifying more complex land use classes (e.g. urban areas, see Supplementary Material 5).

Improving the computation of both *Observables* and *Similarities* should therefore improve the classifications produced at the initial, dichotomous and modular stages. At the initial stage for example, the mapping of clouds and shadows depends on the accuracy of the cloud and cloud-shadow mask implemented previous to SIAM. As for now, we used the algorithm proposed by Hollstein et al. (Hollstein et al., 2016) because it is entirely rule-based and thus in line with the other image processing steps of the system. However, Sanchez et al. (Sanchez et al., 2020) recently compared the efficiency of different algorithms to mask clouds in Sentinel-2 images of the Brazilian Amazon. They especially emphasized the good results achieved by the Fmask method (Qiu et al., 2019) whose potential to significantly improve the initial classification should then be assessed.

At the dichotomous stage, land surfaces are sub-divided in four classes ("Terrestrial Vegetation","Aquatic Vegetation","Water" and"-Mineral") by crossing two binary masks of vegetated and aquatic areas. Whereas this approach was sufficient to monitor the classes of interest for this specific application, it is worth noting that the"Mineral" class is actually implicitly identified since it is defined by combining"Non Aquatic" and"Non Vegetated" areas. Yet, an explicit classification of"Mineral" classes directly based on the occurrences of the"Brown Mineral" class of *Colour-Material* may improve the mapping of land surface material types, also potentially including additional dichotomous classes such as"Aquatic Mineral" corresponding to temporary flooded bare areas (e.g. sandy banks).

At the modular stage, the combination of occurrence classes of *Colour-Material* led to a large number of potential classes (142 identified in the present study). If additional observables (e.g. texture) and similarities (e.g. endmember fractions, patch geometry) were to be computed, this number could even increase dramatically. As a consequence, the automatic definition of IDs, colours and labels for an increasing number of modular classes may become an issue. We suggest the IDs could be handled in bit flag arrays as in the quality assurance data associated with MODIS Land Products (GSFC-NASA, 2020). Bit flag arrays contain multiple flags (e.g. binary values) stored in fixed bit positions of the array depending on the characteristic they measured. The binary strings can then easily be converted in numeric decimal values. With regard to colours, the colour mixing approach based on weighted RGB values as used in this study is somehow simplistic. Additional tests

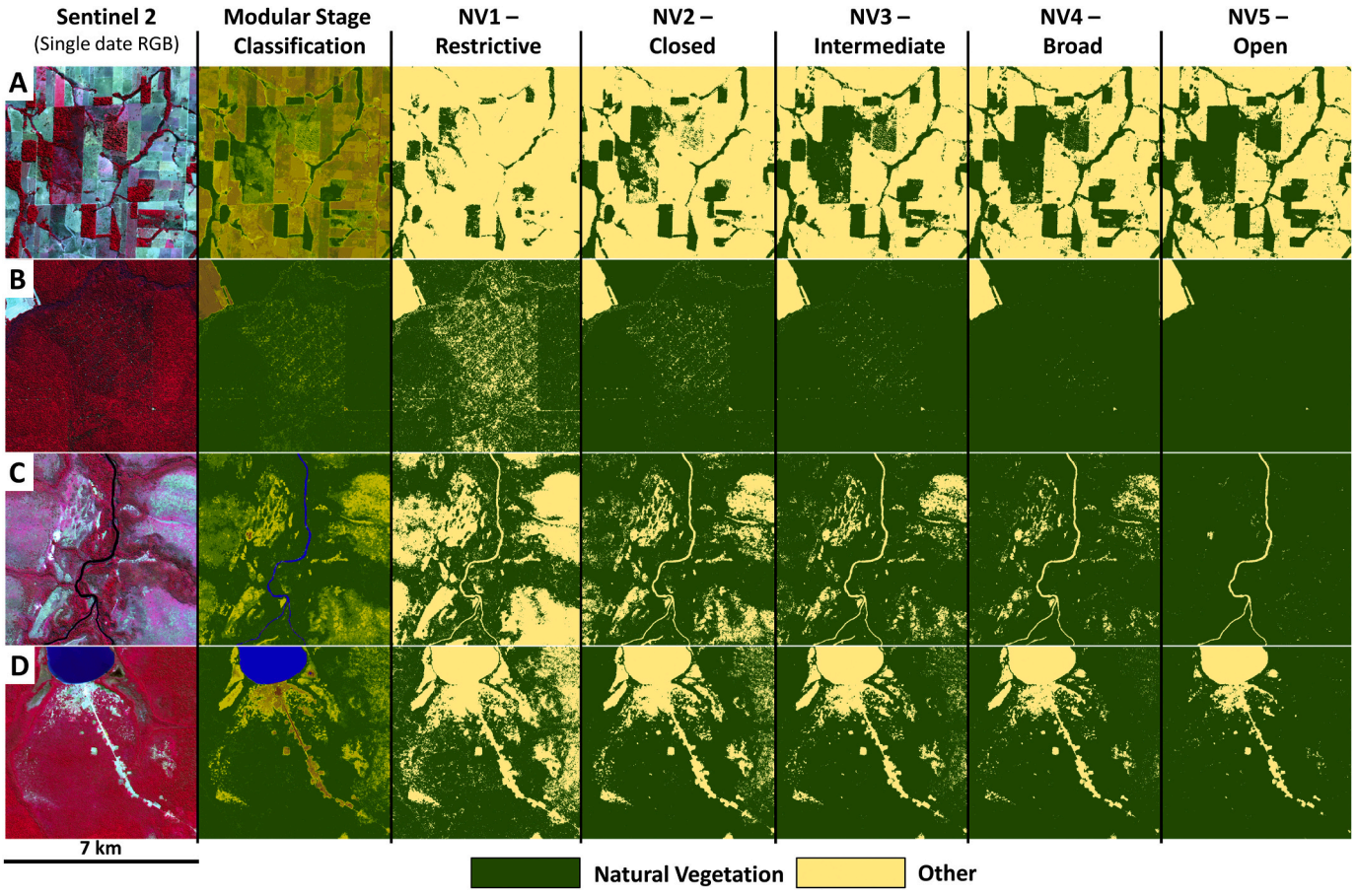

Fig. 17. Examples of classification of woody vegetation according to different thresholds of forest definition for four study cases: A) Degraded forest in a pasture landscape, B) Logged forest, C) Forest-Cerrado transition and D) Indigenous village surrounded by small-scale agriculture.

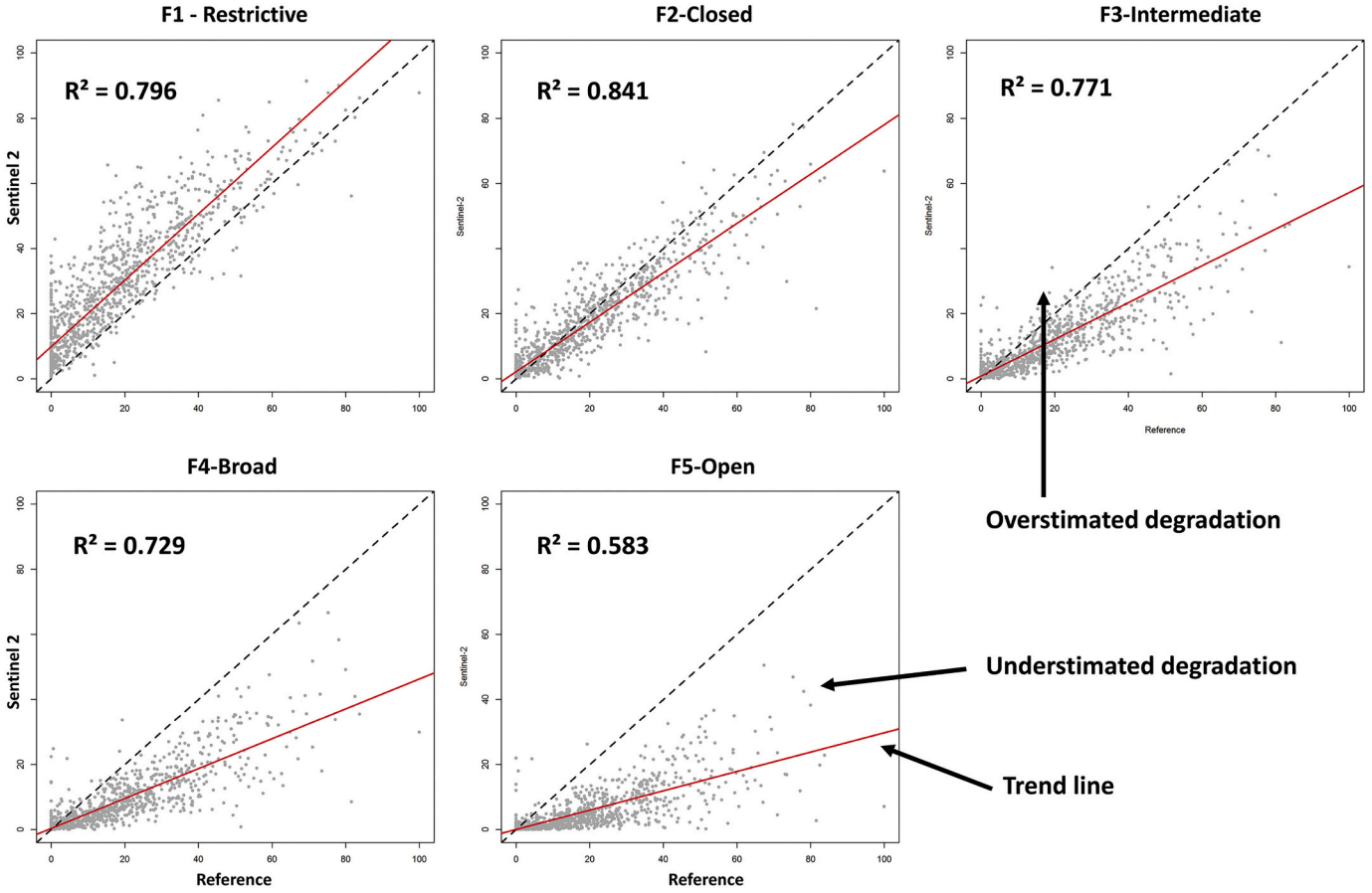

Fig. 18. Correlations between the proportions of degraded riparian forest in $N = 1{,}239$ watersheds as estimated by visual interpretation (Reference data set) and by the Sentinel-2 classification, using various thresholds at the modular stage.

in alternative colour spaces (e.g.HSL and HSB spaces) should be performed to mix colours more closely with the way human vision perceives colours. Yet, the most challenging issue is certainly the non-numeric one, i.e. to improve the description of image pixels and objects with meaningful semantic labels based on natural language terms (Câmara, 2020).

Finally, whereas the effectiveness of the approach was here assessed through traditional statistical indices to validate the accuracy of land cover maps, we wish to emphasize that the resulting classifications may not necessarily be assessed through comparisons with land cover reference samples. For example, ecologists used to process land cover maps to understand the distribution of animal species could run distribution models with various input maps based on different combinations of modular classes in order to identify a range of classes (related to ranges in the vegetation gradient) that best correlates with the presence of that species of interest. By considering numerous low-level symbolic labels describing the spectro-temporal signatures instead of a few arbitrarily-defined high-level thematic land cover classes, it would both reduce the gap between the data and the end-users and avoid overly simplifying representation of reality that may not adequately represent how species perceive their environment (Rocchini et al., 2013; Comber et al., 2005).

5.2. The conceptual framework

A major objective of the approach proposed in this paper was to assess if a well justified and simple rule-based knowledge-driven approach could achieve high scores of classification accuracy. For this reason, we intentionally implemented the current version of the system as a fully knowledge-driven approach relying on threshold-based rule-sets. These thresholds (except for cloud detection whose rules were inspired from (Hollstein et al., 2016)) were defined based on logical considerations. For example, all thresholds in Table 4 were fixed arbitrarily to cover all the gradient from 0 to 100% occurrence, as in other knowledge-driven classification systems such as LCCS or General Habitat Categories (GHC) (Kosmidou et al., 2014). The results obtained for this specific application using Sentinel-2 images of the Southern Brazilian Amazon were encouraging and confirmed the relevance of the approach, especially to monitor vegetation gradients in tropical landscapes of pioneer frontiers. Additional tests (see Supplementary Materials; SM) performed in other study areas in Brazil (SM 2 and 5), France (SM 3), India (SM 4), Indonesia and Congo (SM 6), with other data (Landsat-8) and other classes of interest (i.e. urban areas, urban vegetation, irrigated fields, coniferous forests) also illustrate the potential of the system to compete with more traditional data-driven approaches (SM 2 and 3).

Yet, beyond our intention to test the system for other applications, we also need to discuss further evolution of the conceptual framework.

First, as mentioned previously, the perspective to integrate additional similarities (e.g. about patch geometry) may require moving from a pixel- to an object-based image analysis, thus adopting the GEOBIA principles (Blaschke et al., 2014; Blaschke, 2010). Considering the semantic contraction proposed by Couclelis (Couclelis, 2010), the"field-to-object" transition occurs between the 3rd and 4th steps of the contraction (Table 2), i.e. when fields of properties (i.e. *Observables* and *Similarities*) are used to identify and name simple geographic objects. Moving to a GEOBIA approach would then be an important step towards a full implementation of the semantic contraction. In this regard, the method introduced in this paper may be considered as complementary to the approach described by Lang et al. (Lang et al., 2014) who started from a GEOBIA land use classification to focus on levels 4 to 7 of the

same semantic contraction.

Second, we need to better consider the temporal dimension in the conceptual framework, especially to assess the potential of such knowledge-based approach to monitor fine temporal changes. Kennedy et al. (Kennedy et al., 2014) identified various cases of changes (i.e. abrupt, trend or cyclic changes). Whereas abrupt changes (e.g. land use conversions such as deforestation) should be detectable, we hope that fine land cover modifications can also be evidenced (e.g. as for the logged forest in Fig. 17). Yet, detecting temporal trends and cycles is more complex. In that case, it may be necessary to rely on statistical algorithms to describe and qualify such evolution (e.g."bimodal distribution of Strong Green Vegetation" to characterize double-cropping systems).

Third, although our motivation to continue investigating knowledge-driven approaches remains a priority, it is worth noting that, at a time when machine learning classifiers tend to prevail in remote sensing science, we shall also consider evolving towards an hybrid version of the system combining both knowledge- and data-driven approaches. Indeed, supervised or unsupervised statistical learning classifiers (Mountrakis et al., 2011; Belgiu and Dragut, 2016; Zhu et al., 2017) may be useful to map *Observables* by identifying classes of *Colour-Material* or to categorize *Similarities*. Novel approaches of semantic segmentation based on deep learning algorithms have also been proven to be efficient to delineate and label image objects starting from a pixel-based classification (Kemker et al., 2018). By doing so, the knowledge-driven part of the system would then focus on the articulation of the image characteristics in order to derive the three classification stages.

In this regard, and fourthly, the role of ontologies to formalize and handle symbolic expert knowledge should be crucial (Arvor et al., 2019; Arvor et al., 2013; Claramunt, 2020). To be effective, ontology-based applications must rely on existing framework ontologies such as OBOE as introduced in this paper (Madin et al., 2007). These ontologies are essential since they can be connected to other framework ontologies such as, for example, 1) ontologies dedicated to the representation of spatial relations (Kong et al., 2003) for the purpose of adopting a GEOBIA approach or 2) the Semantic Sensor Network (SSN) ontology that provides a framework to describe sensors and their observations (Compton et al., 2012), thus potentially articulating multisource (e.g. Landsat, MODIS and Sentinel 1) observations in a unique system.

Nonetheless, moving from theory to practice is challenging. Whereas the current method has been entirely implemented in the R environment (R Core Team, 2019), its formal implementation in Semantic Web standards to integrate ontologies is anything but straightforward (Claramunt, 2020). For example, the experiment led by Andrés et al. (Andrés et al., 2017) to reproduce SIAM in an ontology-based system emphasized the difficulty to operationalize image processing tasks with ontologies.

5.3. Improving end-user and remote sensing expert knowledge

Due to these operational limitations, as for now, the main advantage of ontologies may actually lie in its ability to formalize, aggregate and share expert knowledge about the symbolic definitions of land cover classes. This would firstly concern the symbolic descriptions from a remote sensing perspective. For example, similarly to spectral libraries used to store numeric knowledge about spectral signatures of target objects, we argue that our system could serve as a basis to build libraries of symbolic definitions of the representation of land cover classes in remote sensing images. Performing additional tests in other contexts would indeed make it possible to accumulate symbolic definitions of land cover classes in order to build a remote sensing expert knowledge database to be stored in ontologies. For example, if N end-users used the approach to classify"Forests" in N study areas across the world, we could retrieve the N symbolic definitions of the representation of Forests in Sentinel-2 images and store them into ontologies. Then, any new end-user interested in mapping Forests could reuse these ontologies containing the experience of the N first users to derive N maps of'Forests". Such strategy for ontology-building would follow the recommendations of Janowicz (Janowicz, 2012) who argued for "a radical paradigm shift in ontology engineering away from a small number of authoritative, global ontologies developed top-down, to a large number of local ontologies that are driven by application needs and developed bottom-up based on observation data." In this regard, the remote sensing community should benefit from experiences in other scientific communities to build collaborative web-based tools for the construction of thesaurus and ontologies in ecology (Laporte and IsabelleMougenot, 2012) and geosciences (Kalbasi et al., 2013).

On the long term, we consider that aggregating remote sensing expert knowledge in ontologies should improve the interpretability of remote sensing images by facilitating the discovery of relationships between the image characteristics of geographic objects and the real-world characteristics of corresponding geographic entities. For instance, in the present study, occurrences of Green Vegetation *Colour-Material* appeared to be efficient to map dense, evergreen, woody vegetation but limited to map open cerrado areas. In this regard, improving the interpretability of remote sensing images would contribute to reducing the semantic gap between end-users and remote sensing experts.

Finally, the interpretability issue questions the possibility to evolve from a user-adaptive to a user-centered remote sensing. Indeed, if efficiently connected to remote sensing expert knowledge, formal and explicit end-user expert knowledge focused on the definitions/descriptions of real-world geographic entities could drive the interpretation of remote sensing images. For example, end-users interested in mapping dense evergreen forests in other regions of the world than the Amazon may capitalize on the expert knowledge formalized in this study to implement efficient workflow of image processing tasks. Of course, this would first require convincing end-users to explicit and formalize their own conceptualization of land cover classes of interest in order to achieve mapping results that better suits with their requirements. This is the reason why, beyond being useful and effective, such system needs to be primarily usable by end-users, following major principles of user-centered agile software development (Brhel et al., 2015). To do so, we need interactive web-tools to allow the end-users to access and process the maps. For this reason, we are currently implementing the approach in Google Earth Engine and we then intend to develop interactive tools to do the class assignment without any specific geoprocessing skills.

6. Conclusion

We introduced an automatic knowledge-driven methodology to interpret time series of Sentinel-2 images. The method is based on a conceptual framework inspired from ontologies of scientific observations (i.e. the OBOE ontology (Madin et al., 2007)) and ontologies of geographic information (i.e. the semantic contraction introduced by Couclelis (Couclelis, 2010)). We relied on this framework to implement a rule-based system to map forested areas and water bodies on a large area (529,780 km^2, 75 Sentinel-2 tiles) in the Southern Brazilian Amazon as requested by local end-users. The method includes the mapping of characteristics (i.e. *Observables* and *Similarities*) to then derive three classifications, i.e. initial, dichotomous and modular classifications. The accuracy results confirmed the potential of the knowledge-driven approach to monitor vegetation gradients and map water bodies at regional and local scale, taking full advantage of the 10 m spatial resolution.

At a time when data-driven approaches to classify remote sensing images tend to prevail, we consider that the remote sensing community should pay more attention to knowledge-driven approaches since they enable to reduce the gap between the map producers and the end-users. Yet, it implies to formalize both end-user and remote sensing expert knowledge in order to effectively guide the image processing tasks. In this regard, the use of knowledge representation techniques such as

ontologies appears promising, although still challenging to implement operationally.

Data

The 2017 modular classifications can be accessed at: doi: 10.35110/0e3e3a68-871c-4359-9c56-716d4071e992.

Declaration of Competing Interest

The authors declare that they have no known competing financial interests or personal relationships that could have appeared to influence the work reported in this paper.

Acknowledgments

This work was supported by the French National Centre for Space Studies (CNES) through the TOSCA CASTAFIOR project (grant agreement 181670), by the European Union's Horizon 2020 Research and Innovation Program under the Marie Sklodowska Curie grant ODYSSEA (no 691053), by the GUYAMAZON LandCoverMap project (grant agreement 304459/00) and by the French National Centre for Scientific Research (CNRS) through the International Emerging Action SCOLTEL project (grant agreement 231438).

Appendix A. Supplementary data

Supplementary data to this article can be found online at https://doi.org/10.1016/j.rse.2021.112615.

References

Adamo, M., Tomaselli, V., Tarantino, C., Vicario, S., Veronico, G., Lucas, R., Blonda, P., 2020. Knowledge-based classification of grassland ecosystem based on multi-temporal WorldView-2 data and FAO-LCCS taxonomy. Remote Sens. 12, 1447. https://doi.org/10.3390/rs12091447.

Alvarez-Vanhard, E., Houet, T., Mony, C., Lecoq, L., Corpetti, T., 2020. Can uavs fill the gap between in situ surveys and satellites for habitat mapping? Remote Sens. Environ. 243, 111780. https://doi.org/10.1016/j.rse.2020.111780. URL. http://www.sciencedirect.com/science/article/pii/S0034425720301504.

Andrés, S., Arvor, D., Mougenot, I., Libourel, T., Durieux, L., 2017. Ontology-based classification of remote sensing images using spectral rules. Comput. Geosci. 102, 158–166. https://doi.org/10.1016/j.cageo.2017.02.018.

Arvor, D., Jonathan, M., Meirelles, M.S.P., Dubreuil, V., Durieux, L., 2011. Classification of MODIS EVI time series for crop mapping in the state of mato grosso, brazil. Int. J. Remote Sens. 32, 7847–7871. https://doi.org/10.1080/01431161.2010.531783.

Arvor, D., Durieux, L., Andrés, S., Laporte, M.-A., 2013. Advances in geographic object-based image analysis with ontologies: a review of main contributions and limitations from a remote sensing perspective. ISPRS J. Photogramm. Remote Sens. 82, 125–137. https://doi.org/10.1016/j.isprsjprs.2013.05.003.

Arvor, D., Daher, F.R., Briand, D., Dufour, S., Rollet, A.-J., Simões, M., Ferraz, R.P., 2018. Monitoring thirty years of small water reservoirs proliferation in the southern brazilian amazon with landsat time series. ISPRS J. Photogramm. Remote Sens. 145, 225–237. https://doi.org/10.1016/j.isprsjprs.2018.03.015.

Arvor, D., Belgiu, M., Falomir, Z., Mougenot, I., Durieux, L., 2019. Ontologies to interpret remote sensing images: why do we need them? GISci. Rem. Sens. 56, 911–939. https://doi.org/10.1080/15481603.2019.1587890.

Arvor, D., Silgueiro, V., Nunes, G.M., Nabucet, J., Dias, A.P., 2021. The 2008 map of consolidated rural areas in the brazilian legal amazon state of mato grosso: accuracy assessment and implications for the environmental regularization of rural properties. Land Use Policy 103, 105281. https://doi.org/10.1016/j.landusepol.2021.105281.

Asner, G.P., 2001. Cloud cover in landsat observations of the brazilian amazon. Int. J. Remote Sens. 22, 3855–3862. https://doi.org/10.1080/01431160010006926.

Asner, G.P., 2009. Automated mapping of tropical deforestation and forest degradation: CLASlite. J. Appl. Remote. Sens. 3, 033543. https://doi.org/10.1117/1.3223675. URL. http://remotesensing.spiedigitallibrary.org/article.aspx?doi=10.1117/1.3223675.

Baraldi, A., Puzzolo, V., Blonda, P., Bruzzone, L., Tarantino, C., 2006. Automatic spectral rule-based preliminary mapping of calibrated landsat TM and ETM+ images. IEEE Trans. Geosci. Remote Sens. 44, 2563–2586. https://doi.org/10.1109/TGRS.2006.874140. URL. http://ieeexplore.ieee.org/lpdocs/epic03/wrapper.htm?arnumber=1677766.

Baraldi, A., Durieux, L., Simonetti, D., Conchedda, G., Holecz, F., Blonda, P., 2010. Automatic spectral-rule-based preliminary classification of radiometrically calibrated SPOT-4/-5/IRS, AVHRR/MSG, AATSR, IKONOS/QuickBird/OrbView/GeoEye, and DMC/SPOT-1/-2 imagery—part i: System design and implementation. IEEE Trans. Geosci. Remote Sens. 48, 1299–1325. https://doi.org/10.1109/tgrs.2009.2032457.

Bégué, A., Arvor, D., Bellon, B., Betbeder, J., de Abelleyra, D., Ferraz, R.P.D., Lebourgeois, V., Lelong, C., Simões, M., Verón, S.R., 2018. Remote sensing and cropping practices: a review. Remote Sens. 10, 99. https://doi.org/10.3390/rs10010099.

Belgiu, M., Dragut, L., 2016. Random forest in remote sensing: a review of applications and future directions. ISPRS J. Photogramm. Remote Sens. 114, 24–31. https://doi.org/10.1016/j.isprsjprs.2016.01.011. URL. http://www.sciencedirect.com/science/article/pii/S0924271616000265.

Blaschke, T., 2010. Object based image analysis for remote sensing. ISPRS J. Photogramm. Remote Sens. 65, 2–16. https://doi.org/10.1016/j.isprsjprs.2009.06.004.

Blaschke, T., Strobl, J., 2001. What's Wrong with Pixels? Some Recent Developments Interfacing Remote Sensing and Gis.

Blaschke, T., Hay, G.J., Kelly, M., Lang, S., Hofmann, P., Addink, E., Feitosa, R.Q., van der Meer, F., van der Werff, H., van Coillie, F., Tiede, D., 2014. Geographic object-based image analysis – towards a new paradigm. ISPRS J. Photogramm. Remote Sens. 87, 180–191. https://doi.org/10.1016/j.isprsjprs.2013.09.014.

Brhel, M., Meth, H., Maedche, A., Werder, K., 2015. Exploring principles of user-centered agile software development: a literature review. Inf. Softw. Technol. 61, 163–181. https://doi.org/10.1016/j.infsof.2015.01.004.

Bullock, E.L., Woodcock, C.E., Olofsson, P., 2020. Monitoring tropical forest degradation using spectral unmixing and landsat time series analysis. Remote Sens. Environ. 238, 110968. https://doi.org/10.1016/j.rse.2018.11.011.

Büttner, G., 2014. CORINE land cover and land cover change products. In: Land Use and Land Cover Mapping in Europe, Springer Netherlands, pp. 55–74. https://doi.org/10.1007/978-94-007-7969-3_5.

Câmara, G., 2020. On the semantics of big earth observation data for land classification. J. Spat. Inform. Sci. https://doi.org/10.5311/josis.2020.20.645.

Camara, G., Assis, L.F., Ribeiro, G., Ferreira, K.R., Llapa, E., Vinhas, L., 2016. Big earth observation data analytics. In: Proceedings of the 5th ACM SIGSPATIAL International Workshop on Analytics for Big Geospatial Data - BigSpatial 16. ACM Press. https://doi.org/10.1145/3006386.3006393.

Casati, R., 2009. Minor Entities: Surfaces, Holes and Shadows, 36. Routledge Companion to Metaphysics, pp. 382–388.

G. Castilla, G. J. Hay, Image objects and geographic objects, in: Lecture Notes in Geoinformation and Cartography, Springer Berlin Heidelberg, 2020. pp. 91–110. doi: 10.1007/978-3-540-77058-9_5.

CEO, 2018. The CEOS Earth Observation Handbook - Satellite Earth Observation in Support of the Sustainable Development Goals.

Cerbaro, M., Morse, S., Murphy, R., Lynch, J., Griffiths, G., 2020a. Information from earth observation for the management of sustainable land use and land cover in brazil: an analysis of user needs. Sustainability 12, 489. https://doi.org/10.3390/su12020489.

Cerbaro, M., Morse, S., Murphy, R., Lynch, J., Griffiths, G., 2020b. Challenges in using earth observation (EO) data to support environmental management in brazil. Sustainability 12, 10411. https://doi.org/10.3390/su122410411.

Chen, J., Chen, J., Liao, A., Cao, X., Chen, L., Chen, X., He, C., Han, G., Peng, S., Lu, M., Zhang, W., Tong, X., Mills, J., 2015. Global land cover mapping at 30m resolution: a POK-based operational approach. ISPRS J. Photogramm. Remote Sens. 103, 7–27. https://doi.org/10.1016/j.isprsjprs.2014.09.002.

Claramunt, C., 2020. Ontologies for geospatial information: progress and challenges ahead. J. Spat. Inform. Sci. https://doi.org/10.5311/josis.2020.20.666.

Coluzzi, R., Imbrenda, V., Lanfredi, M., Simoniello, T., 2018. A first assessment of the sentinel-2 level 1-c cloud mask product to support informed surface analyses. Remote Sens. Environ. 217, 426–443. https://doi.org/10.1016/j.rse.2018.08.009.

Comber, A., Fisher, P., Wadsworth, R., 2005. You know what land cover is but does anyone else?…an investigation into semantic and ontological confusion. Int. J. Remote Sens. 26, 223–228. https://doi.org/10.1080/0143116042000274032.

Compton, M., Barnaghi, P., Bermudez, L., García-Castro, R., Corcho, O., Cox, S., Graybeal, J., Hauswirth, M., Henson, C., Herzog, A., Huang, V., Janowicz, K., Kelsey, W.D., Phuoc, D.L., Lefort, L., Leggieri, M., Neuhaus, H., Nikolov, A., Page, K., Passant, A., Sheth, A., Taylor, K., 2012. The SSN ontology of the w3c semantic sensor network incubator group, Web Semantics: science. Serv. Agents World Wide Web 17, 25–32. https://doi.org/10.1016/j.websem.2012.05.003.

Congalton, R., Gu, J., Yadav, K., Thenkabail, P., Ozdogan, M., 2014. Global land cover mapping: a review and uncertainty analysis. Remote Sens. 6, 12070–12093. https://doi.org/10.3390/rs61212070. URL. http://www.mdpi.com/2072-4292/6/12/12070/.

Couclelis, H., 1992. People manipulate objects (but cultivate fields): Beyond the raster-vector debate in GIS. In: Theories and Methods of Spatio-Temporal Reasoning in Geographic Space. Springer, Berlin Heidelberg, pp. 65–77. https://doi.org/10.1007/3-540-55966-3_3.

Couclelis, H., 2010. Ontologies of geographic information. Int. J. Geogr. Inf. Sci. 24, 1785–1809. https://doi.org/10.1080/13658816.2010.484392.

Couteron, P., Pelissier, R., Nicolini, E.A., Paget, D., 2005. Predicting tropical forest stand structure parameters from fourier transform of very high-resolution remotely sensed canopy images. J. Appl. Ecol. 42, 1121–1128. https://doi.org/10.1111/j.1365-2664.2005.01097.x.

Cox, S.J.D., 2013. An explicit owl representation of iso/ogc observations and measurements. In: Proceedings of the 6th International Conference on Semantic Sensor Networks - Volume 1063, SSN'13. CEUR-WS.org, Aachen, Germany, Germany, pp. 1–18. URL. http://dl.acm.org/citation.cfm?id=2874543.2874544.

de Almeida, C.A., Coutinho, A.C., Esquerdo, J.C.D.M., Adami, M., Venturieri, A., Diniz, C. G., Dessay, N., Durieux, L., Gomes, A.R., 2016. High spatial resolution land use and land cover mapping of the brazilian legal amazon in 2008 using landsat-5/TM and MODIS data. Acta Amazon. 46, 291–302. https://doi.org/10.1590/1809-4392201505504.

Di Gregorio, A., 2005. Food and Agriculture Organization of the United Nations, United Nations Environment Programme, Land cover classification system: classification concepts and user manual: LCCS, number 8 in Environment and natural resources series, software version 2 ed. Food and Agriculture Organization of the United Nations, Rome.

Falomir, Z., Museros, L., Gonzalez-Abril, L., Sanz, I., 2013. A model for qualitative colour comparison using interval distances. Displays 34, 250–257. https://doi.org/10.1016/j.displa.2013.07.004.

Frantz, D., Haß, E., Uhl, A., Stoffels, J., Hill, J., 2018. Improvement of the fmask algorithm for sentinel-2 images: separating clouds from bright surfaces based on parallax effects. Remote Sens. Environ. 215, 471–481. https://doi.org/10.1016/j.rse.2018.04.046.

Freundschuh, S.M., Egenhofer, M.J., 1997. Human conceptions of spaces: implications for GIS. Trans. GIS 2, 361–375. https://doi.org/10.1111/j.1467-9671.1997.tb00063.x.

Fritz, S., McCallum, I., Schill, C., Perger, C., See, L., Schepaschenko, D., van der Velde, M., Kraxner, F., Obersteiner, M., 2012. Geo-wiki: an online platform for improving global land cover. Environ. Model Softw. 31, 110–123. https://doi.org/10.1016/j.envsoft.2011.11.015.

Fuster, B., Sánchez-Zapero, J., Camacho, F., García-Santos, V., Verger, A., Lacaze, R., Weiss, M., Baret, F., Smets, B., 2020. Quality assessment of PROBA-v LAI, fAPAR and fCOVER collection 300 m products of copernicus global land service. Remote Sens. 12, 1017. https://doi.org/10.3390/rs12061017.

Giri, C., Long, J., 2014. Land cover characterization and mapping of South America for the year 2010 using landsat 30 m satellite data. Remote Sens. 6, 9494–9510. https://doi.org/10.3390/rs6109494. URL. http://www.mdpi.com/2072-4292/6/10/9494/.

Giri, C., Pengra, B., Long, J., Loveland, T., 2013. Next generation of global land cover characterization, mapping, and monitoring. Int. J. Appl. Earth Obs. Geoinf. 25, 30–37. https://doi.org/10.1016/j.jag.2013.03.005.

Gong, P., Wang, J., Yu, L., Zhao, Y., Zhao, Y., Liang, L., Niu, Z., Huang, X., Fu, H., Liu, S., Li, C., Li, X., Fu, W., Liu, C., Xu, Y., Wang, X., Cheng, Q., Hu, L., Yao, W., Zhang, H., Zhu, P., Zhao, Z., Zhang, H., Zheng, Y., Ji, L., Zhang, Y., Chen, H., Yan, A., Guo, J., Yu, L., Wang, L., Liu, X., Shi, T., Zhu, M., Chen, Y., Yang, G., Tang, P., Xu, B., Giri, C., Clinton, N., Zhu, Z., Chen, J., Chen, J., 2013. Finer resolution observation and monitoring of global land cover: first mapping results with Landsat TM and ETM+ data. Int. J. Remote Sens. 34, 2607–2654. https://doi.org/10.1080/01431161.2012.748992.

Gorelick, N., Hancher, M., Dixon, M., Ilyushchenko, S., Thau, D., Moore, R., 2017. Google earth engine: planetary-scale geospatial analysis for everyone. Remote Sens. Environ. 202, 18–27. https://doi.org/10.1016/j.rse.2017.06.031.

Grekousis, G., Mountrakis, G., Kavouras, M., 2015. An overview of 21 global and 43 regional land-cover mapping products. Int. J. Remote Sens. 1–27. https://doi.org/10.1080/01431161.2015.1093195.

Gruber, T.R., 1993. A translation approach to portable ontology specifications. Knowl. Acquis. 5, 199–220. https://doi.org/10.1006/knac.1993.1008. URL. http://linkinghub.elsevier.com/retrieve/pii/S1042814383710083.

GSFC-NASA, 2020. Modis Atmosphere - Bit Interpretation. URL. https://modis-images.gsfc.nasa.gov/tools_bit_interpretation.html. Accessed: 2020-04-23.

Hák, T., Janoušková, S., Moldan, B., 2016. Sustainable development goals: a need for relevant indicators. Ecol. Indic. 60, 565–573. https://doi.org/10.1016/j.ecolind.2015.08.003.

Hansen, M.C., Potapov, P.V., Moore, R., Hancher, M., Turubanova, S.A., Tyukavina, A., Thau, D., Stehman, S.V., Goetz, S.J., Loveland, T.R., Kommareddy, A., Egorov, A., Chini, L., Justice, C.O., Townshend, J.R.G., 2013. High-resolution global maps of 21st-century forest cover change. Science 342, 850–853. https://doi.org/10.1126/science.1244693.

Hollstein, A., Segl, K., Guanter, L., Brell, M., Enesco, M., 2016. Ready-to-use methods for the detection of clouds, cirrus, snow, shadow, water and clear sky pixels in sentinel-2 MSI images. Remote Sens. 8, 666. https://doi.org/10.3390/rs8080666.

Inglada, J., Vincent, A., Arias, M., Tardy, B., Morin, D., Rodes, I., 2017. Operational high resolution land cover map production at the country scale using satellite image time series. Remote Sens. 9, 95. https://doi.org/10.3390/rs9010095.

Jackson, F., 1982. Epiphenomenal qualia. Philos. Q. 32, 127. https://doi.org/10.2307/2960077.

Janowicz, K., 2012. Observation-driven geo-ontology engineering. Trans. GIS 16, 351–374. https://doi.org/10.1111/j.1467-9671.2012.01342.x.

Jensen, J.R., 1983. Biophysical remote sensing. Ann. Assoc. Am. Geogr. 73, 111–132. https://doi.org/10.1111/j.1467-8306.1983.tb01399.x.

Kalbasi, R., Janowicz, K., Reitsma, F., Boerboom, L., Alesheikh, A., 2013. Collaborative ontology development for the geosciences. Trans. GIS 18, 834–851. https://doi.org/10.1111/tgis.12070.

Kalensky, Z., 1998. AFRICOVER land cover database and map of africa. Can. J. Remote. Sens. 24, 292–297. https://doi.org/10.1080/07038992.1998.10855250.

Kemker, R., Salvaggio, C., Kanan, C., 2018. Algorithms for semantic segmentation of multispectral remote sensing imagery using deep learning. ISPRS J. Photogramm. Remote Sens. 145, 60–77. https://doi.org/10.1016/j.isprsjprs.2018.04.014.

Kennedy, R.E., Andréfouët, S., Cohen, W.B., Gómez, C., Griffiths, P., Hais, M., Healey, S. P., Helmer, E.H., Hostert, P., Lyons, M.B., Meigs, G.W., Pflugmacher, D., Phinn, S.R., Powell, S.L., Scarth, P., Sen, S., Schroeder, T.A., Schneider, A., Sonnenschein, R., Vogelmann, J.E., Wulder, M.A., Zhu, Z., 2014. Bringing an ecological view of change to landsat-based remote sensing. Front. Ecol. Environ. 12, 339–346. https://doi.org/10.1890/130066.

Kong, H., Jung, K., Choi, J., Kim, W., Kim, P., Park, J., 2003. Representing the spatial relations in the semantic web ontologies, in: Lecture Notes in Computer Science. Springer, Berlin Heidelberg, pp. 77–87. https://doi.org/10.1007/978-3-540-24581-0_7.

Kosmidou, V., Petrou, Z., Bunce, R.G., Mücher, C.A., Jongman, R.H., Bogers, M.M., Lucas, R.M., Tomaselli, V., Blonda, P., Padoa-Schioppa, E., Manakos, I., Petrou, M., 2014. Harmonization of the land cover classification system (LCCS) with the general habitat categories (GHC) classification system. Ecol. Indic. 36, 290–300. https://doi.org/10.1016/j.ecolind.2013.07.025.

Lang, S., 2008. Object-based image analysis for remote sensing applications: modeling reality – dealing with complexity. In: Lecture Notes in Geoinformation and Cartography. Springer, Berlin Heidelberg, pp. 3–27. https://doi.org/10.1007/978-3-540-77058-9_1.

Lang, S., Kienberger, S., Tiede, D., Hagenlocher, M., Pernkopf, L., 2014. Geons – domain-specific regionalization of space. Cartogr. Geogr. Inf. Sci. 41, 214–226. https://doi.org/10.1080/15230406.2014.902755.

Laporte, M.-A., IsabelleMougenot, E., 2012. Garnier, ThesauForm—traits: a web based collaborative tool to develop a thesaurus for plant functional diversity research. Ecol. Inform. 11, 34–44. https://doi.org/10.1016/j.ecoinf.2012.04.004.

Lee, J.S., Pottier, E., 2009. Polarimetric radar imaging: From basics to applications, 2009, Optical Science and Engineering.

Lin, S., Li, J., Liu, Q., Li, L., Zhao, J., Yu, W., 2019. Evaluating the effectiveness of using vegetation indices based on red-edge reflectance from sentinel-2 to estimate gross primary productivity. Remote Sens. 11, 1303. https://doi.org/10.3390/rs11111303.

Lu, D., 2003. Linear mixture model applied to amazonian vegetation classification. Remote Sens. Environ. 87, 456–469. https://doi.org/10.1016/j.rse.2002.06.001.

Lu, D., 2005. Aboveground biomass estimation using landsat TM data in the brazilian amazon. Int. J. Remote Sens. 26, 2509–2525. https://doi.org/10.1080/01431160500142145.

Lucas, R., Rowlands, A., Brown, A., Keyworth, S., Bunting, P., 2007. Rule-based classification of multi-temporal satellite imagery for habitat and agricultural land cover mapping. ISPRS J. Photogramm. Remote Sens. 62, 165–185. https://doi.org/10.1016/j.isprsjprs.2007.03.003.

Lucas, R., Blonda, P., Bunting, P., Jones, G., Inglada, J., Arias, M., Kosmidou, V., Petrou, Z.I., Manakos, I., Adamo, M., Charnock, R., Tarantino, C., Mücher, C.A., Jongman, R.H., Kramer, H., Arvor, D., Honrado, J.P., Mairota, P., 2015. The earth observation data for habitat monitoring (EODHaM) system. Int. J. Appl. Earth Obs. Geoinf. 37, 17–28. https://doi.org/10.1016/j.jag.2014.10.011. URL. http://linkinghub.elsevier.com/retrieve/pii/S0303243414002347.

Madin, J., Bowers, S., Schildhauer, M., Krivov, S., Pennington, D., Villa, F., 2007. An ontology for describing and synthesizing ecological observation data. Ecol. Inform. 2, 279–296.

Madin, J.S., Bowers, S., Schildhauer, M.P., Jones, M.B., 2008. Advancing ecological research with ontologies. Trends Ecol. Evol. 23, 159–168.

Marcus, G., 2018. Deep Learning: A Critical Appraisal arXiv:arXiv:1801.00631.

Mark, D.M., 1993. Toward a theoretical framework for geographic entity types. In: Lecture Notes in Computer Science. Springer, Berlin Heidelberg, pp. 270–283. https://doi.org/10.1007/3-540-57207-4_18.

Martins, V.S., Novo, E.M., Lyapustin, A., Aragão, L.E., Freitas, S.R., Barbosa, C.C., 2018. Seasonal and interannual assessment of cloud cover and atmospheric constituents across the amazon (2000–2015): insights for remote sensing and climate analysis. ISPRS J. Photogramm. Remote Sens. 145, 309–327. https://doi.org/10.1016/j.isprsjprs.2018.05.013.

Mountrakis, G., Im, J., Ogole, C., 2011. Support vector machines in remote sensing: a review. ISPRS J. Photogramm. Remote Sens. 66, 247–259. https://doi.org/10.1016/j.isprsjprs.2010.11.001.

Pekel, J.-F., Cottam, A., Gorelick, N., Belward, A.S., 2016. High-resolution mapping of global surface water and its long-term changes. Nature 540, 418–422. https://doi.org/10.1038/nature20584.

Picoli, M.C.A., Camara, G., Sanches, I., Simões, R., Carvalho, A., Maciel, A., Coutinho, A., Esquerdo, J., Antunes, J., Begotti, R.A., Arvor, D., Almeida, C., 2018. Big earth observation time series analysis for monitoring brazilian agriculture. ISPRS J. Photogramm. Remote Sens. 145, 328–339. https://doi.org/10.1016/j.isprsjprs.2018.08.007.

S. Qiu, Z. Zhu, B. He, Fmask 4.0: improved cloud and cloud shadow detection in landsats 4–8 and sentinel-2 imagery, Remote Sens. Environ. 231 (2019) 111205. doi: 10.1016/j.rse.2019.05.024.

R Core Team, 2019. R: A Language and Environment for Statistical Computing. R Foundation for Statistical Computing, Vienna, Austria. URL. http://www.R-project.org/.

Rocchini, D., Foody, G.M., Nagendra, H., Ricotta, C., Anand, M., He, K.S., Amici, V., Kleinschmit, B., Förster, M., Schmidtlein, S., Feilhauer, H., Ghisla, A., Metz, M., Neteler, M., 2013. Uncertainty in ecosystem mapping by remote sensing. Comput. Geosci. 50, 128–135. https://doi.org/10.1016/j.cageo.2012.05.022. URL. http://linkinghub.elsevier.com/retrieve/pii/S0098300412001781.

Roitman, I., Vieira, L.C.G., Jacobson, T.K.B., da Cunha Bustamante, M.M., Marcondes, N. J.S., Cury, K., Estevam, L.S., da Costa Ribeiro, R.J., Ribeiro, V., Stabile, M.C., de Miranda Filho, R.J., Avila, M.L., 2018. Rural environmental registry: an innovative model for land-use and environmental policies. Land Use Policy 76, 95–102. https://doi.org/10.1016/j.landusepol.2018.04.037.

Sachs, J.D., 2012. From millennium development goals to sustainable development goals. Lancet 379, 2206–2211. https://doi.org/10.1016/s0140-6736(12)60685-0.

Sack, R.D., 2010. A concept of physical space in geography. Geogr. Anal. 5, 16–34. https://doi.org/10.1111/j.1538-4632.1973.tb00994.x.

Sanchez, A., Picoli, M., Camara, G., Andrade, P., Chaves, M., Lechler, S., Soares, A., Marujo, R., Simões, R., Ferreira, K., Queiroz, G., 2020. Comparison of cloud cover detection algorithms on Sentinel–2 images of the Amazon tropical forest. Remote Sens. 12, 1284. https://doi.org/10.3390/rs12081284. URL. https://www.mdpi.com/2072-4292/12/8/1284.

Sano, E.E., Ferreira, L.G., Asner, G.P., Steinke, E.T., 2007. Spatial and temporal probabilities of obtaining cloud-free landsat images over the brazilian tropical savanna. Int. J. Remote Sens. 28, 2739–2752. https://doi.org/10.1080/01431160600981517.

See, L., Mooney, P., Foody, G., Bastin, L., Comber, A., Estima, J., Fritz, S., Kerle, N., Jiang, B., Laakso, M., Liu, H.-Y., Milčinski, G., Nikšič, M., Painho, M., Pődör, A., Olteanu-Raimond, A.-M., Rutzinger, M., 2016. Crowdsourcing, citizen science or volunteered geographic information? the current state of crowdsourced geographic information. ISPRS Int. J. Geo Inf. 5, 55. https://doi.org/10.3390/ijgi5050055.

Small, C., 2020. Grand challenges in remote sensing image analysis and classification. Front. Rem. Sens. https://doi.org/10.3389/frsen.2020.605220.

Smeulders, A.W.M., Worring, M., Santini, S., Gupta, A., Jain, R., 2000. Content-based image retrieval at the end of the early years. IEEE Trans. Pattern Anal. Mach. Intell. 22, 1349–1380.

Souza, C., Kirchhoff, F., Oliveira, B., Ribeiro, J., Sales, M., 2019. Long-term annual surface water change in the brazilian amazon biome: potential links with deforestation, infrastructure development and climate change. Water 11, 566. https://doi.org/10.3390/w11030566.

Souza, Carlos M., Shimbo, Julia Z., Rosa, Marcos R., Parente, Leandro R., Alencar, Ane A., Rudorff, Bernardo F.T., Hasenack, Heinrich, Matsumoto, Marcelo, Ferreira, Laerte G., Souza-Filho, Pedro W.M., de Oliveira, Sergio W., Rocha, Washington F., Fonseca, Antonio V., Marques, Camila B., Diniz, Cesar G., Costa, Diego, Monteiro, Dyeden, Rosa, Eduardo R., Velez-Martin, Eduardo, Weber, Eliseu J., Lenti, Felipe E.B., Paternost, Fernando F., Pareyn, Frans G.C., Siqueira, Joao V., Viera, Jose L., Ferreira Neto, Luiz C., Saraiva, Marciano M., Sales, Marcio H., Salgado, Moises P.G., Vasconcelos, Rodrigo, Galano, Soltan, Mesquita, Vinicius V., Azevedo, Tasso, 2020. Reconstructing Three Decades of Land Use and Land Cover Changes in Brazilian Biomes with Landsat Archive and Earth Engine. Remote Sensing 12 (17), 2735. https://doi.org/10.3390/rs12172735.

Sprugel, D.G., 1991. Disturbance, equilibrium, and environmental variability: What is 'natural' vegetation in a changing environment? Biol. Conserv. 58, 1–18. https://doi.org/10.1016/0006-3207(91)90041-7.

Stickler, C.M., Nepstad, D.C., Azevedo, A.A., McGrath, D.G., 2013. Defending public interests in private lands: compliance, costs and potential environmental consequences of the brazilian forest code in mato grosso. Philosoph. Trans. Royal Soc. B: Biol. Sci. 368, 20120160. https://doi.org/10.1098/rstb.2012.0160.

Sudmanns, M., Tiede, D., Augustin, H., Lang, S., 2019. Assessing global sentinel-2 coverage dynamics and data availability for operational earth observation (EO) applications using the EO-compass. Int. J. Digital Earth 13, 768–784. https://doi.org/10.1080/17538947.2019.1572799.

Taniwaki, R.H., Forte, Y.A., Silva, G.O., Brancalion, P.H., Cogueto, C.V., Filoso, S., Ferraz, S.F., 2018. The native vegetation protection law of brazil and the challenge for first-order stream conservation. Perspect. Ecol. Conserv. 16, 49–53. https://doi.org/10.1016/j.pecon.2017.08.007.

Turner, B.L., Lambin, E.F., Reenberg, A., 2007. The emergence of land change science for global environmental change and sustainability. Proc. Natl. Acad. Sci. 104, 20666–20671. https://doi.org/10.1073/pnas.0704119104.

Voudouris, V., 2010. Towards a unifying formalisation of geographic representation: the object–field model with uncertainty and semantics. Int. J. Geogr. Inf. Sci. 24, 1811–1828. https://doi.org/10.1080/13658816.2010.488237.

Waldner, F., Canto, G.S., Defourny, P., 2015. Automated annual cropland mapping using knowledge-based temporal features. ISPRS J. Photogramm. Remote Sens. 110, 1–13. https://doi.org/10.1016/j.isprsjprs.2015.09.013. URL. http://linkinghub.elsevier.com/retrieve/pii/S0924271615002233.

Zhu, X.X., Tuia, D., Mou, L., Xia, G., Zhang, L., Xu, F., Fraundorfer, F., 2017. Deep Learning in Remote Sensing: A Comprehensive Review and List of Resources. CoRR abs/1710.03959 5 (4), 8–36. https://doi.org/10.1109/MGRS.2017.2762307.

Zhu, Z., Wang, S., Woodcock, C.E., 2015. Improvement and expansion of the fmask algorithm: cloud, cloud shadow, and snow detection for landsats 4–7, 8, and sentinel 2 images. Remote Sens. Environ. 159, 269–277. https://doi.org/10.1016/j.rse.2014.12.014.

Zhu, Z., Wulder, M.A., Roy, D.P., Woodcock, C.E., Hansen, M.C., Radeloff, V.C., Healey, S.P., Schaaf, C., Hostert, P., Strobl, P., Pekel, J.-F., Lymburner, L., Pahlevan, N., Scambos, T.A., 2019. Benefits of the free and open landsat data policy. Remote Sens. Environ. 224, 382–385. https://doi.org/10.1016/j.rse.2019.02.016.